Editors' Suggestion

The sixteenfold way and the quantum Hall effect at half-integer filling factors

Ken K. W. Ma and D. E. Feldman
Department of Physics, Brown University, Providence, Rhode Island 02912, USA

(Received 15 April 2019; published 3 July 2019)

Fractional quantum Hall states at half-integer filling factors have been observed in many systems beyond the $\frac{5}{2}$ and $\frac{7}{2}$ plateaus in GaAs quantum wells. This includes bilayer states in GaAs, several half-integer plateaus in ZnO-based heterostructures, and quantum Hall liquids in graphene. In all cases, Cooper pairing of composite fermions is believed to explain the plateaus. The nature of Cooper pairing and the topological order on those plateaus are hotly debated. Different orders are believed to be present in different systems. This makes it important to understand experimental signatures of all proposed orders. We review the expected experimental signatures for all possible composite-fermion states at half-integer filling. We address Mach-Zehnder interferometry, thermal transport, tunneling experiments, and Fabry-Pérot interferometry. For this end, we introduce a uniform description of the topological orders of Kitaev's sixteenfold way in terms of their wave functions, effective Hamiltonians, and edge theories.

DOI: 10.1103/PhysRevB.100.035302

I. INTRODUCTION

Experimental discovery of the fractional quantum Hall effect (FQHE) [1] has started a new chapter in condensed matter physics and opened the field of topological matter. One major development was the observation of a quantized Hall plateau at the filling factor $\nu = \frac{5}{2}$ [2,3]. This has led to many innovative theoretical ideas. One of them is non-Abelian statistics of elementary excitations [4–7] which may open a path to topological quantum computing [8,9]. Another related idea is topological superconductivity [10–12].

A powerful approach to quantum Hall physics involves composite fermions [13]. In particular, odd-denominator FQHE can be understood as the integer quantum Hall effect of composite fermions. Such an explanation fails for half-integer states, where composite fermions are subject to zero effective magnetic field. Instead, a gapped half-integer liquid can be seen as a superconductor built from Cooper pairs of composite fermions [14].

Different pairing channels give rise to different topological orders. The correspondence is not one to one. Indeed, pairing can occur in an infinite number of angular momentum channels. At the same time, topological order depends only on the types of anyons in the system and their mutual statistics. Kitaev's classification [15] reveals 16 possibilities. Understanding which ones are relevant for available materials has proved a major challenge.

The bilayer state at $\nu = \frac{1}{2}$ in GaAs [16,17] is believed to be the Abelian 331 liquid [18–21]. The nature of the single-layer $\frac{5}{2}$ liquid in GaAs remains controversial. The existing experimental results are consistent with the non-Abelian PH-Pfaffian liquid [22–27] at charge densities $n \sim 2$–3×10^{11} cm^{-2}. Yet, numerics [28–33] supports the non-Abelian Pfaffian [4] and anti-Pfaffian orders [25,34]. Besides, some experiments [35–37] were interpreted as compatible with the Abelian 113 and 331 states [18,38,39]. To make matters even more puzzling, experimental evidence [40,41] exists for a different topological order at low-electron densities $n < 0.5 \times 10^{11}$ cm^{-2}. Little is known about the fragile $\frac{7}{2}$ state in GaAs [42,43] and several recently discovered half-integer states in ZnO [44,45]. It was argued that the SU(2)$_2$ topological order is present in graphene [46,47]. A recent thermal conductance experiment [48] also supports a topological order from Kitaev's classification in the spin-liquid material α-RuCl$_3$. Thus, several of the 16 theoretical possibilities are currently seen as viable candidates for real materials. Not enough evidence exists to dismiss the remaining orders of Kitaev's sixteenfold way. This makes it crucial to understand possible experimental signatures of all 16 orders and provides the main motivation for this paper.

Not all available experimental probes are equally useful to distinguish the 16 topological orders. For example, the quasiparticle charge of $e/4$ was reported by several groups on the $\frac{5}{2}$ plateau in GaAs [35–37,49–54]. This does not shed light on the topological order since the same quasiparticle charge is predicted in all 16 states. Similarly, the preponderance of the experimental evidence [55–59] points at a spin-polarized FQHE liquid in GaAs at $n \sim 2$–3×10^{11} cm^{-2}. All 16 topological orders are compatible with a fully polarized liquid. One can get more information from quasiparticle tunneling [35–38,54,60,61], thermal conductance [14,62–65], upstream noise experiments [66–71], and interferometry [9,52,72–94]. These are the types of experiments we consider below. Interferometry in the Mach-Zehnder geometry [95] exhibits particularly interesting behavior.

Kitaev's classification addresses a neutral system, such as a spin liquid [15]. Its extension to a charged FQHE system involves subtleties which we handle below. A simultaneous discussion of 16 topological orders requires their uniform description. Simple wave functions are known for some of the orders, such as Pfaffian [4] and PH-Pfaffian [24]. We use the known wave functions for the Pfaffian and 113 states to generate similar wave functions for all other topological orders. This is possible due to mother-daughter relations among all

non-Abelian states and among all Abelian states. The same mother-daughter relations give a simple way to construct edge theories for all 16 orders and to iteratively generate effective Hamiltonians in a coupled-stripe construction. Coupled-wire constructions have already been used for half-integer states [96–98]. Our iterative approach is different.

The paper is organized as follows. In Sec. II, we begin by introducing our construction of topological orders for half-integer FQH liquids. In particular, we formulate mother-daughter relations among the orders and show a way to systematically generate wave functions for multiple orders. Then, in Sec. III, we show explicitly that the resulting topological orders satisfy the sixteenfold way. Based on this result, we address multiple experimental signatures of all orders in Secs. IV, V, and VI. The physics of Mach-Zehnder interferometry is especially rich and subtle. Its discussion occupies Sec. V, with the more technical points being addressed in the Appendix. We summarize experimental signatures in Table VI in Sec. VI. In Sec. VII, we relate different topological orders iteratively and construct their effective Hamiltonians from a system of coupled quantum Hall stripes in the Pfaffian state. Any other topological order of the sixteenfold way could also be used as a starting point instead of the Pfaffian order. We conclude our work in Sec. VIII.

II. TOPOLOGICAL ORDERS OF THE SIXTEEN FOLD WAY

We focus on an FQHE system with a filling factor $\nu = n + \frac{1}{2}$, where n is an integer. In the simplest picture, n filled spin-resolved Landau levels do not affect topological properties; FQHE physics is due to one half-filled spin-resolved Landau level. It is unclear if such picture captures the relevant microscopic physics. For example, Coulomb interaction of electrons in different Landau levels is strong in GaAs at $\nu = \frac{5}{2}$. This results in Landau-level mixing (LLM) effects [29–32,99–102]. In a uniform system without LLM, Pfaffian, and anti-Pfaffian FQHE liquids have exactly the same energy [25,34]. Arbitrarily weak LLM breaks this degeneracy. Moreover, it was argued that strong LLM can help stabilize the PH-Pfaffian order [24,103]. The above picture also assumes a single-component (in particular, spin-polarized) wave function. The existing evidence does support spin-polarized half-integer states in ZnO [44] and in GaAs [55–58] at the electron densities $n \sim 2$–3×10^{11} cm^{-2}. At the same time, the accepted description of the $\frac{1}{2}$ state in bilayers assumes a two-component wave function with equal populations of the two layers [18].

The above points reflect great difficulty of writing a realistic wave function for an experimentally relevant system. This difficulty becomes even more daunting if one attempts to incorporate disorder effects. Such effects are present in all samples and may be crucial for the nature of topological order [24,104–107]. On the other hand, if the topological order is known, much of the physics does not depend on the details of the wave function. Thus, it is useful to have simple representative wave functions for each of the 16 topological orders of the sixteenfold way. Such trial wave functions have been written for some of the orders, for example, Pfaffian [4]. As we will see, very similar trial wave functions emerge for all other composite fermion orders in half-integer FQHE. Of course, their construction sheds no light on which order is present in any given experimental system. This question can only be answered in a laboratory. In Secs. IV and V, we address the relevant experimental signatures in detail.

In what follows, we will focus on the simplest setting of a single half-filled spin-polarized Landau level $\nu = \frac{1}{2}$. Any disorder and LLM effects are neglected. The only exception will be the PH-Pfaffian wave function which greatly simplifies in a system with Landau-level mixing.

Wave functions of electrons in the lowest Landau level are significantly constrained by the analyticity requirement [108]. They can be represented as

$$\Psi(z_1, \ldots, z_N) = \Phi(z_1, \ldots, z_N) \exp\left(-\sum_{i=1}^{N} \frac{|z_i|^2}{4l_B^2}\right), \quad (1)$$

where $z_k = x_k + iy_k$ are the positions of N electrons, l_B is the magnetic length, and $\Phi(z_1, \ldots, z_N)$ is a holomorphic function. We will choose a polynomial Φ. The polynomial is homogeneous since the degree of each monomial is proportional to the angular momentum. A single-electron wave function with $\Phi(z) \sim z^k$ describes charge density concentrated along a ring of radius $r \sim \sqrt{k}$ [109]. Hence, the polynomial $\Phi(z_1, \ldots, z_N)$ describes electrons on a disk of radius $R \sim \sqrt{k_{\max}}$, where $k_{\max}$ is the highest power of z_i in Φ. The total degree $k = \sum k_i$ of each monomial $z_1^{k_1} \ldots z_N^{k_N}$ in Φ satisfies the relation $k \approx N^2/[2\nu]$.

This leads us to another constraint that the wave function should produce the correct charge density. At $\nu = \frac{1}{2}$, the simplest choice, compatible with the correct density, is $\Phi(z_1, \ldots, z_N) = \Phi_{\text{flux}} = \Pi_{i<j}(z_i - z_j)^2$. This yields an acceptable wave function for bosons but not for electrons. To fix the statistics, Φ_{flux} must be multiplied by an antisymmetric factor $\Phi_{\text{cf}}(z_1, \ldots, z_N)$. To maintain the correct density in the thermodynamic limit $N \to \infty$, the factor should change the degree k of Φ by $o(N^2)$.

The two factors Φ_{flux} and Φ_{cf} have a natural interpretation in the composite fermion picture [13]. Note that experimental evidence exists for composite fermions at $\nu = \frac{5}{2}$ in GaAs [58,110]. The former factor Φ_{flux} describes two flux quanta attached to each electron. The resulting composite fermions move in a zero effective magnetic field. Their wave function is Φ_{cf}. It describes Cooper pairing of composite fermions. The most famous example is p-wave pairing in the Pfaffian state [14,111–113]. A trial wave function takes the form

$$\text{Pf}\left(\frac{1}{z_i - z_j}\right) \prod_{i<j} (z_i - z_j)^2 \exp\left(-\sum_{i=1}^{N} \frac{|z_i|^2}{4l_B^2}\right), \quad (2)$$

with $\Phi_{\text{cf}} = \text{Pf}(\frac{1}{z_i - z_j})$. As was observed by Moore and Read [4], the above choice of the bulk wave function determines the nature of the gapless edge modes. There are two of them: a charged boson and a neutral Majorana fermion.

In general, pairing between composite fermions can be described by an effective Bardeen-Cooper-Schrieffer (BCS) mean-field Hamiltonian. For spinless fermions, we have

$$H_{\text{BCS}} = \sum_{\mathbf{k}} \left[\xi_{\mathbf{k}} c_{\mathbf{k}}^\dagger c_{\mathbf{k}} + \frac{1}{2}(\Delta_{\mathbf{k}}^* c_{-\mathbf{k}} c_{\mathbf{k}} + \Delta_{\mathbf{k}} c_{\mathbf{k}}^\dagger c_{-\mathbf{k}}^\dagger)\right]. \quad (3)$$

Here, $\xi_{\mathbf{k}} = \frac{k^2}{2m} - \mu$, with m and μ labeling the effective mass of a composite fermion and the chemical potential of the system, respectively. The fermionic creation operator $c^\dagger_{\mathbf{k}}$ and destruction operator $c_{\mathbf{k}}$ satisfy the anticommutation relation $\{c_{\mathbf{k}}, c^\dagger_{\mathbf{k}'}\} = \delta_{\mathbf{k},\mathbf{k}'}$. The pairing function is denoted as $\Delta_{\mathbf{k}}$. When $\mu > 0$, the system is in the weak-pairing phase [14]. In Ref. [114], Dubail and Read modeled the gap function for the complex l-wave pairing as $\Delta_{\mathbf{k}} = \tilde{\Delta}(k_x \pm ik_y)^l$. By analyzing the entanglement spectrum in some specific cases, they showed that this kind of pairing between spinless fermions should lead to l chiral Majorana fermions at the edge.

The edge structure establishes the connection of wave functions with Kitaev's sixteenfold way. As shown by Kitaev [15], different topological orders in topological superconductors of composite fermions differ by the number of Majorana modes on the edge. Moreover, since the bulk is gapped, the universal low-energy physics is determined by the edge structure. As a consequence, all experimental probes, addressed in this paper, involve edge physics. Thus, we begin our discussion of topological orders with a review of their edge structures. This will uncover mother-daughter relations between various orders and will allow us to generate relevant wave functions in a straightforward way.

A. Mother-daughter relations for non-Abelian orders

As shown by Wen and Zee [60,115], an Abelian topological order for a fractional quantum Hall state can be characterized by a K matrix and a charge vector t. Although the Pfaffian order is non-Abelian, one can view it as a direct product between $\mathrm{SU}(2)_2$ Ising anyon and an Abelian U(1) bosonic sector. The latter is characterized by a 1×1 matrix $K = (2)$ and $t = 1$, so that $\nu = t^T K^{-1} t = \frac{1}{2}$. The K matrix determines the Abelian modes on the edge. In particular, their number equals the dimension of the matrix. Thus, the Pfaffian edge contains only one Abelian Bose mode, in addition to a Majorana fermion from the Ising sector. The direction of those modes is determined by the sign of the magntic field and is called "downstream." We will generally assume that downstream is counterclockwise [116].

To generate a chain of topological orders, we particle-hole (PH) conjugate [25,34] the Pfaffian order. On the edge, this means reversing the direction of all Bose and Majorana edge modes (downstream → upstream) and adding an integer downstream Bose mode. We obtain the anti-Pfaffian order with an upstream Majorana and a 2×2 diagonal K matrix encoding two Abelian modes: $K_{11} = 1, K_{22} = -2$. The charge vector $t = (1, 1)^T$. In terms of edge physics, the first element of the charge vector corresponds to the contribution from the $\nu = 1$ edge and the second element comes from the reversed $\nu = \frac{1}{2}$ FQHE edge. We denote the two corresponding charged modes as $\{\phi_0, \phi_1\}$. Disorder on the edge equilibrates the two modes. The appropriate language for edge physics involves then two linear combinations of $\phi_{0,1}$: an overall charged mode that propagates downstream and a neutral upstream boson [25,34]. Specifically, we consider a change of the basis $(\phi_\rho, \phi_n)^T = W(\phi_0, \phi_1)^T$. The K matrix and the charge vector transform as

$$K \to (W^{-1})^T K W^{-1}, \quad t \to (W^{-1})^T t. \tag{4}$$

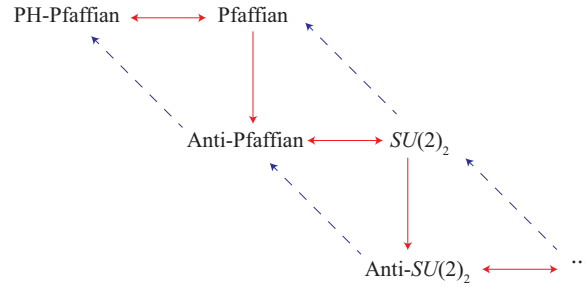

FIG. 1. Illustration of generating non-Abelian topological orders for the $\nu = \frac{5}{2}$ fractional quantum Hall state by particle-hole conjugation (vertical arrows) and neutral-mode flipping (horizontal arrows). The topological orders can be related iteratively via a coupled-stripe construction in Sec. VII. The red solid lines correspond to the first construction (CW1) and the blue dashed lines correspond to the second construction (CW2).

One can easily check that the filling factor ν is invariant under the transformation. The W matrix in this case is given by

$$W = \begin{pmatrix} 1 & 1 \\ 1 & 2 \end{pmatrix}. \tag{5}$$

The transformed K matrix is diagonal with $K_{11} = 2$, $K_{22} = -1$, and the charge vector becomes $t = (1, 0)^T$.

Our second trick is flipping the neutral modes. Indeed, the $\mathrm{SU}(2)_2$ edge structure can be obtained by flipping the directions of the neutral modes (Majorana fermion ψ and the bosonic mode ϕ_n). As a result, ψ and ϕ_n get the same downstream chirality as ϕ_ρ. The flipping of the bosonic neutral mode corresponds to changing the sign of K_{22}: $-1 \to 1$. This trick can also be seen as negative-flux attachment [117].

By repeating the above processes, a chain of non-Abelian topological orders can be generated iteratively as shown in Fig. 1. The K matrices for the topological orders obtained with particle-hole conjugation are diagonal with $K_{11} = 1$, $K_{22} = -2$, and $K_{ii} = -1$ ($i \geqslant 3$), the charge vector being $t = (1, 1, 0, \ldots, 0)^T$. We rewrite the K matrices in the basis of a single downstream charged mode and multiple upstream neutral modes. This is achieved by using the following W matrix:

$$W = \begin{pmatrix} 1 & 1 & 0 & 0 & \ldots & 0 & 0 \\ 1 & 2 & 0 & 0 & \ldots & 0 & 0 \\ 0 & 0 & 1 & 0 & \ldots & 0 & 0 \\ \vdots & \vdots & \vdots & \vdots & \ddots & \vdots & \vdots \\ 0 & 0 & 0 & 0 & \ldots & 1 & 0 \\ 0 & 0 & 0 & 0 & \ldots & 0 & 1 \end{pmatrix}. \tag{6}$$

With the transformation from Eq. (4), the K matrix transforms into

$$K = \begin{pmatrix} 2 & 0 & 0 & \ldots & 0 \\ 0 & -1 & 0 & \ldots & 0 \\ 0 & 0 & -1 & \ldots & 0 \\ \vdots & \vdots & \vdots & \ddots & \vdots \\ 0 & 0 & 0 & \ldots & -1 \end{pmatrix}. \tag{7}$$

Here, the negative sign indicates that all neutral modes have opposite chirality with respect to the charged mode. This gives

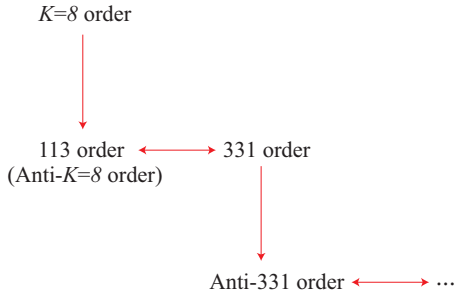

FIG. 2. Illustration of generating Abelian topological orders by particle-hole conjugation (vertical arrows) and neutral-mode flipping (horizontal arrows). It is reminded that the spin-polarized 113 order is topologically equivalent to the anti-$K = 8$ state [39]. The topological orders can be related iteratively with the coupled-stripe construction of Sec. VII.

a natural description of a disorder-dominated phase [118]. To flip all the bosonic neutral modes, one simply changes all negative matrix elements from -1 to 1.

B. Mother-daughter relations for Abelian orders

Using the techniques of the previous subsection, a chain of Abelian topological orders can also be generated. As illustrated in Fig. 2, we start with the $K = 8$ state to obtain the anti-$K = 8$ state by particle-hole conjugation. Note that the edge modes of the anti-$K = 8$ state cannot be equilibrated by weak disorder in the $T \to 0$ limit [39].

The polarized version of the 113 order is topologically equivalent to the anti-$K = 8$ state [39]. Neutral-mode flipping produces the 331 order from the 113 order. Then, the anti-331 order [38] can be obtained by particle-hole conjugation. As in the non-Abelian case, the K matrices can be diagonalized in the form (7) with the corresponding charge vector $t = (1, 0, \ldots, 0)^T$.

C. Construction of wave functions

One curious aspect of the existing proposals for quantum Hall states at half-integer filling factors is a great diversity of their names: Pfaffian, anti-Pfaffian, 331, $SU(2)_2$, $K = 8$, and so on. This diversity reflects a great variety of the methods used to introduce those topological orders. The 331 state was discovered with a generalization of the Laughlin wave function for two flavors of electrons [18]; the Pfaffian state emerged from a connection with a conformal field theory (CFT) [4]; $SU(2)_2$ was introduced with a parton construction [119]; $K = 8$ can be understood as a quantum Hall state of bosons [115]; the anti-Pfaffian topological order was obtained with particle-hole conjugation [25,34]. Yet, the connection with the sixteenfold way shows that all those orders are close relatives. This is reflected by the mother-daughter relations between the orders. Below we will use those relations to generate a wave function for each order in a systematic way.

The structure of the wave functions will also motivate the prescription for finding allowed quasiparticle types and their mutual statistics. The prescription assumes that a CFT describes the edge of the system. An operator or operators are selected to describe electrons in CFT [120]. All possible quasiparticles correspond to other CFT operators whose operator product expansions (OPE) with the electron operators are single valued.

This prescription is broadly used, but its justification is not obvious. Indeed, the edges of realistic systems are never described by a CFT because different edge modes have different velocities, and numerous irrelevant and sometimes even relevant perturbations enter the Hamiltonian. In our case, the prescription will be placed on a firmer footing by the analysis of bulk wave functions for excited states. Of course, the best proof of the prescription consists in verifying that it reproduces the properties of the sixteenfold way. We confirm that in the next section.

We begin with non-Abelian states and briefly extend our arguments to the Abelian case. As is customary, we consider wave functions in the first Landau level. Any such wave function is the product of an analytic function with the exponential factor $\exp(-\sum_i |z_i|^2/4l_B^2)$ [108]. We generate wave functions in an iterative way. The iterative procedure involves neutral-mode flipping and particle-hole conjugation. We illustrate these two tricks with constructions of the PH-Pfaffian and anti-Pfaffian liquids from the Pfaffian state.

The wave function of the Pfaffian state is well known:

$$\Psi_{\mathrm{Pf}}(\{z_i\}) = \mathrm{Pf}\left\{\frac{1}{z_i - z_j}\right\}\prod_{i<j}(z_i - z_j)^2 \exp\left(-\sum_i |z_i|^2/4l_B^2\right), \tag{8}$$

where $z_k = x_k + iy_k$ is the position of an electron, and l_B is the magnetic length. The complex analytic factor can be reinterpreted as a correlation function $G = \langle \Pi \Psi_k \hat{O}\rangle$ of the electron operators $\Psi_k = \psi(z_k)\exp[2i\phi(z_k)]$ in the conformal field theory [4] with the Lagrangian density

$$\mathcal{L} = \frac{2}{4\pi}[i\partial_y\phi\partial_x\phi + (\partial_x\phi)^2] + \psi(\partial_y - i\partial_x)\psi, \tag{9}$$

where y plays the role of the imaginary time; the operator $\hat{O}$ is localized far away from the system and compensates the electrical charge to ensure that the correlation function of the fields $\exp(2i\phi)$ is nonzero.

The CFT interpretation makes it easy to identify quasiparticles. We define wave functions of excited states as correlation functions $G_q = \langle \Pi \Psi_k \hat{q}(\xi_0)\rangle$, where $\hat{q}$ creates a quasiparticle (from now on we ignore the neutralizing operator $\hat{O}$). $\hat{q}$ is constructed from the operators of the CFT (9). For example, the twist field σ of the Majorana part of the CFT corresponds to $\hat{q} = \sigma\exp(i\omega\phi)$. The parameter ω determines the charge of the excitation. It can be found from the requirement that the wave function is a single-valued function of the electron positions. This identifies $\omega = 1/2 + n$ and the quasiparticle charge is $e/4 + ne/2$.

The PH-Pfaffian wave function is obtained with the help of complex conjugation of the Pfaffian factor in (8). This structure of the wave function reflects a close connection with the Pfaffian order. For example, all density-density correlations are exactly the same for the Pfaffian and PH-Pfaffian wave functions since the absolute values of the wave functions coincide.

The resulting wave function Ψ_{PH} is no longer holomorphic and hence does not describe electrons in a single Landau level. Given strong LLM in realistic systems, this does not create a

problem. Nevertheless, it is important for us to discuss how wave functions can be transformed into a holomorphic form. This involves projection to the lowest Landau level [24]:

$$\Psi_{\rm PH} \to \int \{d^2\xi_i\} \langle \{z_i\} | \{\xi_i\} \rangle \Psi_{\rm PH}(\{\xi_i\}), \tag{10}$$

where $\langle \{z_i\} | \{\xi_i\} \rangle = \Pi_i \exp[-(|\xi_i|^2 - 2\bar{\xi}_i z_i + |z_i|^2)/4l_B^2]$, and the bar denotes complex conjugation. The wave function before projection can be understood as a correlation function of the CFT that differs from (9) by the opposite sign in front of $i\partial_x$ in the Majorana part of the action. This corresponds to neutral-mode flipping or, alternatively, negative-flux attachment. Excited states can again be represented in terms of the correlation functions with the insertion of quasiparticle operators. One can also multiply the wave function by a real rotationally invariant function $R(\{\xi_i\})$ of the coordinates before the projection to the lowest Landau level. This is not expected to affect topological properties. Physically allowed quasiparticles can be found from the single valuedness of the wave function before the lowest Landau level projection. Indeed, the integral (10) is not well defined, if $\Psi_{\rm PH}(\{\xi_i\})$ is not single valued.

Recent numerical work [121] suggests that the simplest projection procedure generates a gapless state from $\Psi_{\rm PH}$. One possibility is that a factor $R(\{\xi_i\})$ should be introduced before projection. Another possibility is that LLM is essential for maintaining a gap in the PH-Pfaffian liquid.

The CFT prescription [120] assumes that the ground-state wave functions it generates are separated by a gap from all excitations. This assumption is plausible and is supported by several well-understood examples. Nevertheless, it can only be proven by identifying a Hamiltonian for which the CFT-generated wave function is the gapped ground state. This explains the importance of Sec. VII below, where we use the same mother-daughter relations as in this section to generate effective Hamiltonians for all topological orders of the sixteenfold way. We are working on an extension of our approach to translationally invariant Hamiltonians.

The role of the particle-hole (PH) symmetry in the PH-Pfaffian state is another subtlety. The PH-Pfaffian topological order is consistent with the PH symmetry, but it is not protected by that symmetry, and so the corresponding ground-state wave functions do not have to be particle-hole symmetric. Moreover, it was argued [103] that a PH-symmetric wave function, which would naturally emerge in Son's picture of massless Dirac fermions, must be gapless. A gapped state with the PH-Pfaffian order requires massive Dirac fermions [103]. This means the absence of the microscopic PH symmetry.

The transition from the Pfaffian to PH-Pfaffian state is a template for neutral-mode flipping in our construction of wave functions for all topological orders. We start with a wave function of the form $\Psi_{\rm unflipped} = \Pi_{i<j}(z_i - z_j)^2 \Psi_{\rm neutral}(\{z_i\})$. The flipped wave function is obtained by the complex conjugation of the expression for $\Psi_{\rm neutral}$: $\Psi_{\rm flipped} = \Pi_{i<j}(z_i - z_j)^2 \bar{\Psi}_{\rm neutral}(\{z_i\})$. If the resulting wave function remains nonanalytic after the removal of the exponential factor $\exp(-\sum_i |z_i|^2/4l_B^2)$, it has to be projected to the lowest Landau level. Particle-hole conjugation is somewhat trickier. We illustrate it with the transition from the Pfaffian to anti-Pfaffian order.

The particle-hole conjugate wave function [25]

$$\begin{aligned}\Psi_{\rm aP}(\{z_i\}) &= \int \{d^2\xi_i\} \bar{\Psi}_{\rm Pf}(\{\xi_i\}) \prod_{i<j}(\xi_i - \xi_j) \prod_{i<j}(z_i - z_j) \prod_{i,j}(\xi_i - z_j) \\ &\quad \times \exp\left(-\sum_i |\xi_i|^2/4l_B^2\right) \exp\left(-\sum_i |z_i|^2/4l_B^2\right),\end{aligned} \tag{11}$$

where the Vandermonde factor $V = \Pi_{i<j}(\xi_i - \xi_j)\Pi_{i<j}(z_i - z_j)\Pi_{i,j}(\xi_i - z_j)$ expresses the wave function of a filled Landau level. Since the filling factor is $\frac{1}{2}$, the numbers of the z_i and ξ_i variables are the same. We rewrite the Vandermonde factor as

$$\begin{aligned}V &= \prod_{i<j}(\xi_i - \xi_j)^2 \prod_{i<j}(z_i - z_j)^2 \frac{\prod_{i,j}(\xi_i - z_j)}{\prod_{i<j}(\xi_i - \xi_j)\prod_{i<j}(z_i - z_j)} \\ &= \prod_{i<j}(\xi_i - \xi_j)^2 \prod_{i<j}(z_i - z_j)^2 |C|^2 \\ &\quad \times \frac{\prod_{i<j}(\bar{\xi}_i - \bar{\xi}_j)\prod_{i<j}(\bar{z}_i - \bar{z}_j)}{\prod_{i,j}(\bar{\xi}_i - \bar{z}_j)},\end{aligned} \tag{12}$$

where $C = \frac{\prod_{i,j}(\xi_i - z_j)}{\prod_{i<j}(\xi_i - \xi_j)\prod_{i<j}(z_i - z_j)}$. Thus,

$$\begin{aligned}\Psi_{\rm aP} = \int \{d^2\xi_i\} |R|^2 &\left[{\rm Pf}\left\{\frac{1}{\bar{\xi}_i - \bar{\xi}_j}\right\}\right] \\ &\times \left[\frac{\prod_{i<j}(\bar{\xi}_i - \bar{\xi}_j)\prod_{i<j}(\bar{z}_i - \bar{z}_j)}{\prod_{i,j}(\bar{\xi}_i - \bar{z}_j)}\right]\left[\prod_{i<j}(z_i - z_j)^2\right],\end{aligned} \tag{13}$$

where the real factor $|R^2| = |C|^2 \Pi_{i<j}|\xi_i - \xi_j|^4 \exp[-\sum_i (2|\xi_i|^2 + |z_i|^2)/4l_B^2]$ ensures convergence and is not expected to influence topological properties of the wave function. Each term in the square brackets in Eq. (13) can be understood as a correlation function of a conformal field theory. The Pfaffian term in the first square brackets is a correlator of the antiholomorphic Majorana fermions ψ. The quadratic term in the third square brackets is a correlation function of the Bose fields $\exp(2i\phi)$ in the theory with $\mathcal{L} = \frac{2}{4\pi}[i\partial_y\phi\partial_x\phi + (\partial_x\phi)^2]$. The middle term is the correlation function $\langle \Pi \exp[i\theta(\xi_m)] \Pi \exp[-i\theta(z_n)] \rangle$ in the antiholomorphic theory with $\mathcal{L} = \frac{1}{4\pi}[-i\partial_y\theta\partial_x\theta + (\partial_x\theta)^2]$. Thus, the topological properties of the wave function are encoded in the correlator

$$\begin{aligned}G_{\rm aP} = \Big\langle &\prod_m \psi(\xi_m) \exp[i\theta(\xi_m)] \\ &\times \prod_n \exp[-i\theta(z_n)] \exp[2i\phi(z_n)] \Big\rangle.\end{aligned} \tag{14}$$

The insertion of a quasiparticle operator into the above correlation function must yield a single-valued function of ξ_m and z_n. Consider an operator $\hat{q} = \sigma \exp(i\omega_1\theta)\exp(i\omega_2\phi)$. Single valuedness with respect to ξ fixes $\omega_1 = 1/2 + n_1$. Hence, single valuedness with respect to z implies $\omega_2 = 1/2 + n_2$. This, of course, agrees with the standard prescription for quasiparticles (cf. Sec. III).

Equations (11)–(14) set a template for particle-hole conjugation in our construction. The key step is the transformation (12) which allows expressing the wave function via a correlator of the type (14).

One can now repeat neutral-mode flipping and particle-hole conjugation in turn a desired number of times to generate wave functions for the eight non-Abelian orders. In such iterative procedure, the projection to the lowest Landau level should only be performed once on the last step, if the wave function does not become holomorphic after the removal [122] of $\exp(-\sum_i |z_i|^2/4l_B^2)$. For example, an $SU(2)_2$ wave function is produced from $\Psi_{\rm aP}$ by neutral-mode flipping; an anti-$SU(2)_2$ wave function is produced by additional particle-hole conjugation; and so on.

The approach to the Abelian orders is the same. Thus, all that is left to do is to specify the wave function for the mother state. The $K = 8$ state is best understood as a quantum Hall state of bosons [115]. For that reason, we use the 113 state as the mother topological order. A convenient wave function for that order can be found in the Supplemental Material for Ref. [39]:

$$\Psi_{113} = \int \prod \{d^2\xi_i\} \Big[\prod_{i<j} (\bar{\xi}_i - \bar{\xi}_j)^4 \prod_{i,j} (\xi_i - z_j)^2 \times \prod_{i<j} (z_i - z_j) \, |R_{113}|^2 \Big], \tag{15}$$

where the real factor $|R_{113}|^2$ ensures convergence. This wave function corresponds to the hierarchical construction with the K matrix

$$K = \begin{pmatrix} 1 & 2 \\ 2 & -4 \end{pmatrix}.$$

We rewrite the complex factor in Eq. (15) as

$$\begin{aligned} &\prod_{i<j} (\bar{\xi}_i - \bar{\xi}_j)^4 \prod_{i,j} (\xi_i - z_j)^2 \prod_{i<j} (z_i - z_j) \\ &= \frac{\prod_{i<j} (\bar{\xi}_i - \bar{\xi}_j)^4 \prod_{i<j} (\bar{z}_i - \bar{z}_j)}{\prod_{i,j} (\bar{\xi}_i - \bar{z}_j)^2} \prod_{i<j} (z_i - z_j)^2 \\ &\times \prod_{i,j} |\xi_i - z_j|^4 \prod_{i<j} |z_i - z_j|^{-2}. \end{aligned} \tag{16}$$

The real factor in the third line is not expected to affect topological properties. The second line can be understood as the correlation function $\langle \Pi \exp[2i\theta(\xi_m)] \Pi \exp[-i\theta(z_n)] \exp[2i\phi(z_n)] \rangle$ in the theory with the Lagrangian density

$$\mathcal{L} = \frac{2}{4\pi} [i\partial_y \phi \partial_x \phi + (\partial_x \phi)^2] + \frac{1}{4\pi} [-i\partial_y \theta \partial_x \theta + (\partial_x \theta)^2]. \tag{17}$$

Quasiparticle operators $\hat{q} = \exp(i\omega_1 \theta) \exp(i\omega_2 \phi)$ must have single-valued OPE with $\exp(2i\theta)$ and $\exp(-i\theta) \exp(2i\phi)$. The first condition allows $\omega_1 = \pm \frac{1}{2}$. The second condition then fixes $\omega_2 = 1/2 + n$. This corresponds to the quasiparticle charge $e/4 + ne/2$. Again, the results agree with the standard prescription.

The 331 order can next be obtained with neutral-mode flipping along the same lines as in the non-Abelian case; the anti-331 order can be obtained from the 331 wave function with particle-hole conjugation; and so on.

D. Quasiparticle operators

Based on the diagonal K matrix in Eq. (7) and the t vector or, alternatively, on the edge theories of the preceding subsection, it is straightforward to determine the scaling dimensions for different types of quasiparticles. Here, we separately discuss the non-Abelian orders and the Abelian orders.

A note about notations. In the previous subsection, we did not explicitly consider edge theories with more than two Bose modes, and we used the notations θ and ϕ for the modes. In this section, we will need multiple edge modes. We will denote all Bose fields as $\phi_{\rm index}$, where index $= \rho$ for the charged mode, and index $= n_i$ or simply i for a neutral mode, where $i = 1, \ldots, N$ numbers the Bose neutral modes. To label topological orders, we will use the Chern number $\nu_C = (2N + m_\psi)C$, where $m_\psi = 0$ for the Abelian orders, $m_\psi = 1$ for the non-Abelian orders, and $C = +1/-1$ for the orders with downstream/upstream neutral modes.

1. Non-Abelian orders

The simplest edge theory for the order with the Chern number ν_C has the Lagrangian density

$$\begin{aligned} \mathcal{L}_{\nu_C} = &- \frac{2}{4\pi} \partial_x \phi_\rho (\partial_t + v_\rho \partial_x) \phi_\rho + i\psi (\partial_t + v_n \mathrm{sign}[\nu_C] \partial_x) \psi \\ &- \frac{1}{4\pi} \sum_{i=1}^{N} \partial_x \phi_i (\mathrm{sign}[\nu_C] \partial_t + v_n \partial_x) \phi_i. \end{aligned} \tag{18}$$

For non-Abelian orders, the most relevant operator for electron takes the following form:

$$\Psi_e = e^{2i\phi_\rho} e^{\pm i\phi_{n_j}} \quad \text{or} \quad \Psi_e = \psi e^{2i\phi_\rho}. \tag{19}$$

Here, the subscript j runs from 1 to N, where N is the number of neutral bosonic modes on the edge. For $e/2$ and $e/4$ quasiparticles, the operators are determined by requiring them to be local with all possible electronic operators. Hence, the most relevant operators for such quasiparticles are

$$\Psi_{e/2} = e^{i\phi_\rho}, \quad \Psi_{e/4} = \sigma e^{i\phi_\rho/2} \prod_{i=1}^{N} e^{\pm i\phi_{n_j}/2}. \tag{20}$$

The twist field σ has the conformal dimension [123] $h_\sigma = \frac{1}{16}$ and satisfies the fusion rule $\sigma \times \sigma = \psi + I$. Therefore, we determine the scaling dimensions for each type of quasiparticles [38,61] as

$$\Delta_e = 3/2, \quad \Delta_{e/2} = 1/4, \quad \Delta_{e/4} = (N+1)/8. \tag{21}$$

From Eq. (21), it is noticed that the $e/4$-quasiparticle operator is the most relevant among all above operators at $N < 1$ (PH-Pfaffian and Pfaffian orders). For $N = 1$, the $e/4$ and $e/2$ quasiparticles are equally relevant [anti-Pfaffian and $SU(2)_2$ orders]. For $N > 1$, the $e/2$ quasiparticle becomes the most relevant [example: anti-$SU(2)_2$ order].

Note that different electron operators (19) do not anticommute. This can be fixed by introducing Klein factors. We will

not explicitly include them in the equations below since they are of little importance to our calculations.

2. Abelian orders

The simplest edge theory for the order with the Chern number ν_C has the Lagrangian density

$$\mathcal{L}_{\nu_C} = -\frac{2}{4\pi}\partial_x\phi_\rho(\partial_t + v_\rho\partial_x)\phi_\rho - \frac{1}{4\pi}\sum_{i=1}^{N}\partial_x\phi_i(\mathrm{sign}[\nu_C]\partial_t + v_n\partial_x)\phi_i. \quad (22)$$

For Abelian orders, the Ising anyonic sector is absent. Therefore, the most relevant electronic operator (except in the $K = 8$ state) takes the following form:

$$\Psi_e = e^{2i\phi_\rho}e^{\pm i\phi_{n_j}}. \quad (23)$$

For $e/2$ and $e/4$ quasiparticles, the most relevant operators are now given by

$$\Psi_{e/2} = e^{i\phi_\rho}, \quad \Psi_{e/4} = e^{i\phi_\rho/2}\prod_{i=1}^{N}e^{\pm i\phi_{n_j}/2}. \quad (24)$$

As a result, the scaling dimensions for each type of quasiparticles are determined [38,61] as

$$\Delta_e = 3/2, \quad \Delta_{e/2} = 1/4, \quad \Delta_{e/4} = N/8 + 1/16. \quad (25)$$

From Eq. (25), we conclude that the $e/4$ quasiparticle is the most relevant for topological orders with $N \leqslant 1$ ($K = 8$, 113, and 331 orders). For $N > 1$, the $e/2$ quasiparticle is the most relevant (example: anti-331 order). Electrons are gapped in the $K = 8$ state. The charge $q = ne/4$ excitation is described by $\Psi_q = \exp(in\phi_\rho)$.

III. FRACTIONAL STATISTICS

After generating different topological orders for the $\nu = \frac{5}{2}$ FQH state in the previous section, we would like to check that all of them are connected with Kitaev's sixteenfold way [15]. Our present goal is twofold. First, we would like to describe quasiparticle statistics for all orders from the previous section. This is needed for the analysis of experimental probes. In the process, we achieve the second goal: explicitly observe a connection of all orders with Kitaev's classification.

In Kitaev's original proposal, all particles are neutral. Hence, we need to separate the neutral and charged sectors of the theory. Thanks to a simple form of the K matrix in Eq. (7), this task is not hard. The only charged field is ϕ_ρ. As far as the contributions of the neutral fields to quasiparticle operators are concerned, there are three different classes of particles: the vacuum (I) class of the particles whose operators contain only ϕ_ρ, the fermion (ε) class in which the charged part is multiplied by an operator with Fermi statistics, and the vortex (σ) class. The products of charged fields and neutral Bose operators are included in the (I) class. Every quasiparticle operator is a product of some exponent of the form $\exp(is\phi_\rho)$, and a "neutralized" part. We identify the neutralized $e/4$ quasiparticles and the neutralized electron as the vortex and the fermion, respectively. Following Ref. [15], the Chern number ν_C is defined as the net number of the Majorana fermions moving downstream. Since each neutral bosonic mode can be fermionized and split into two Majorana fermions, each downstream Bose mode contributes 2 to the Chern number ν_C, and each upstream Bose mode contributes -2.

A. Sixteenfold way for Abelian topological orders

We introduce operators of neutral fermions

$$\varepsilon = \prod_{i=1}^{N}e^{in_i\phi_i}, \quad (26)$$

where we label neutral Bose fields as ϕ_i. Physically, these operators are the neutral parts of various electron operators. Furthermore, n_i is a set of integers which satisfies

$$\sum_{i=1}^{N}n_i \equiv 1 \,(\mathrm{mod}\ 2). \quad (27)$$

We identify vortices σ as the neutral parts of the $e/4$-quasiparticle operators:

$$\sigma = \prod_{i=1}^{N}e^{i(\frac{1}{2}+l_i)\phi_i}. \quad (28)$$

Two vortices are said to be of the same type if they differ by an even number of fermions (equivalently, a boson). Otherwise, they are different types of vortices.

1. Topological spin

We start with computing the topological spin of the fermion and the vortex separately. Following the convention in Ref. [15], we define the topological spin of a particle a as

$$\vartheta_a = e^{2\pi i(h_a - \bar{h}_a)}. \quad (29)$$

The symbols h_a and $\bar{h}_a$ denote the holomorphic and antiholomorphic conformal dimensions of the operator for the particle, respectively. Physically, the topological spin is directly related with the phase θ_a induced from exchanging two identical particles as

$$e^{i\theta_a} = \vartheta_a. \quad (30)$$

Consider first the case of a positive Chern number ν_C. Since the K matrix has been diagonalized in Sec. II, the conformal dimension of a holomorphic vertex operator $V = e^{i\sum_i\alpha_i\phi_i}$ is

$$h = \sum_i (K_{i+1\,i+1})^{-1}\left(\frac{\alpha_i^2}{2}\right) = \sum_i\frac{\alpha_i^2}{2}. \quad (31)$$

Here, $K_{i+1\,i+1} = 1$ is the diagonal matrix element, corresponding to the ith neutral mode ϕ_i. The same exactly scaling dimension $\bar{h}$ is obtained as a function of $\{\alpha_i\}$ for an antiholomorphic vertex operator $V = e^{i\sum_i\alpha_i\phi_i}$ in a theory with a negative Chern number.

Based on the definition in Eq. (29), the topological spin of ε in Eq. (26) is evaluated as

$$\vartheta_\varepsilon = \exp\left[i\,\mathrm{sgn}(\nu_C)\pi\sum_{i=1}^{N}n_i^2\right] = \exp\left[i\,\mathrm{sgn}(\nu_C)\pi\sum_{i=1}^{N}n_i\right] = -1. \quad (32)$$

For σ, the topological spin is determined as

$$\begin{aligned}\vartheta_\sigma &= \exp\left[i\pi\ \mathrm{sgn}(\nu_C)\sum_{i=1}^{N}\left(\frac{1}{2}+l_i\right)^2\right]\\ &= e^{i\pi\ \mathrm{sgn}(\nu_C)N/4}\exp\left[i\pi\ \mathrm{sgn}(\nu_C)\sum_{i=1}^{N} l_i(l_i+1)\right]\\ &= e^{i\pi\nu_C/8}\end{aligned} \tag{33}$$

since $l_i(l_i+1)$ is even for any integer l_i. Therefore, both ϑ_ε and ϑ_σ agree with the results by Kitaev [15].

2. Fusion rules

Kitaev's fusion rules between a vortex and a fermion are satisfied automatically due to our definition of the two different types of vortices. Now, we show that the fusion rules for vortices can be grouped into two different cases. The result of fusing two vortices is given by

$$\sigma_1 \times \sigma_2 \sim \prod_{i=1}^{N} e^{i(1+l_i+m_i)\phi_i}. \tag{34}$$

To determine the nature of the resulting particle, we evaluate its topological spin. From Eq. (29), we have

$$\vartheta = \exp\left[i\pi\sum_{i=1}^{N}(1+l_i+m_i)^2\right] = \exp\left[i\pi\sum_{i=1}^{N}(1+l_i+m_i)\right]. \tag{35}$$

If σ_1 differs from σ_2 by a boson, then $\sum_{i=1}^{N}(l_i+m_i)$ is an even integer. Hence, $\vartheta = e^{iN\pi}$. For odd N, $\vartheta=-1$ which indicates that σ_1 and σ_2 fuse to a fermion. On the other hand, $\vartheta=1$ when N is even. Hence, the two vortices fuse to a boson. In summary, we have

$$\begin{aligned}\sigma\times\sigma &= \varepsilon \quad (\text{when } N \text{ is odd}),\\ \sigma\times\sigma &= I \quad (\text{when } N \text{ is even}).\end{aligned} \tag{36}$$

When σ_1 and σ_2 are two different types of vortices, then $\sum_{i=1}^{N}(l_i+m_i)$ becomes an odd integer. In this case, we have the following fusion rules:

$$\begin{aligned}\sigma_1\times\sigma_2 &= I \quad (\text{when } N \text{ is odd}),\\ \sigma_1\times\sigma_2 &= \varepsilon \quad (\text{when } N \text{ is even}).\end{aligned} \tag{37}$$

For the Abelian topological orders proposed in Sec. II, all neutral modes have the same chirality. Hence, the Chern number satisfies $|\nu_C| = 2N$. The cases of odd N and even N correspond to $\nu_C \equiv 2\,(\mathrm{mod}\ 4)$ and $\nu_C \equiv 0\,(\mathrm{mod}\ 4)$, respectively. One can easily check that the fusion rules in Eqs. (36) and (37) agree with Kitaev's results.

3. Braiding rules

The phase accumulated from exchanging two identical particles can be determined from Eqs. (30), (32), and (33). In our discussion of interferometry, a slightly different phase is essential. We define ϕ_c^{ab} as the phase, accumulated by a particle of type a making a full counterclockwise circle [116] about a particle of type b. The two particles are in the fusion channel c. At $a=b$ one gets

$$\phi_I^{\varepsilon\varepsilon} = 2\theta_\varepsilon = 0, \tag{38}$$

$$\phi_c^{\sigma_1\sigma_1} = \phi_c^{\sigma_2\sigma_2} = 2\theta_\sigma = \frac{\pi\nu_C}{4}\ (\mathrm{mod}\ 2\pi). \tag{39}$$

For nonidentical particles, the exchange phase is not uniquely defined. For this reason, at $a\neq b$, we only consider the encircling phases ϕ_c^{ab}. Let the neutral parts of the particles be described by the vertex operators $V_a = e^{i\sum_i l_i\phi_i}$ and $V_b = e^{i\sum_j m_j\phi_j}$. Since the K matrix is diagonal, the correlation function for the two particles (and a distant additional vertex to ensure a nonzero answer) in the edge CFT is

$$\langle V_a(z)V_b(w)\rangle = (z-w)^{\sum_{i=1}^{N}\frac{l_i m_i}{K_{i+1\,i+1}}}. \tag{40}$$

Thus,

$$\phi_c^{ab} = 2\pi\sum_{i=1}^{N}\frac{l_i m_i}{K_{i+1\,i+1}}\ (\mathrm{mod}\ 2\pi). \tag{41}$$

Moving a fermion around a vortex. Consider encircling a vortex by a fermion. This process induces the phase

$$\begin{aligned}\phi_c^{\sigma\varepsilon} &= 2\pi\ \mathrm{sgn}(\nu_C)\sum_{i=1}^{N} n_i\left(\frac{1}{2}+l_i\right)\ (\mathrm{mod}\ 2\pi)\\ &= \pi\ \mathrm{sgn}(\nu_C)\sum_{i=1}^{N} n_i\ (\mathrm{mod}\ 2\pi)\\ &= \pi.\end{aligned} \tag{42}$$

In the last step, we used the fact that $\sum_i n_i$ is odd since ε is a fermion. Compare this with the rules from Tables 2 and 3 in Ref. [15], which are summarized as follows:

$$\begin{aligned}&\nu_C \equiv 0, 8\ (\mathrm{mod}\ 16): R_m^{ee}=R_e^{\epsilon m}=1,\ R_e^{m\epsilon}=R_m^{\epsilon e}=-1,\\ &\nu_C \equiv \pm 4\ (\mathrm{mod}\ 16): R_m^{ee}=R_m^{\epsilon e}=R_e^{\epsilon m}=R_e^{m\epsilon}=e^{i\pi\nu_C/8},\\ &\nu_C \equiv \pm 2\ (\mathrm{mod}\ 4): R_{\bar a}^{a\epsilon}=R_{\bar a}^{\epsilon a}=R_a^{\bar a\epsilon}=R_a^{\epsilon\bar a}=e^{-i\pi\nu_C/4}.\end{aligned} \tag{43}$$

For all three cases, the phase factor accumulated by a fermion on a complete circle around σ equals

$$R^{\sigma\epsilon}R^{\epsilon\sigma} = -1. \tag{44}$$

This is consisent with the π phase (42).

Moving vortices. Since the topological spin for the vortex agrees with Ref. [15], the phase (33) induced from exchanging two identical vortices must be consistent with the braiding rules from Ref. [15]. Furthermore, the same phase is induced if one of the vortices differs from the other by a boson.

When the difference between the vortices is a fermion, the phase induced by moving one of them around the other is

$$\begin{aligned}\phi_c^{\sigma_1\sigma_2} &= 2\pi\,\mathrm{sgn}(\nu_C)\sum_{i=1}^{N}\left(\frac{1}{2}+l_i\right)\left(\frac{1}{2}+m_i\right)\ (\mathrm{mod}\ 2\pi)\\ &= \left(\frac{\pi\nu_C}{4}+\pi\right)\ (\mathrm{mod}\ 2\pi).\end{aligned} \tag{45}$$

The corresponding braiding rules in Ref. [15] are

$$\begin{aligned}
&\nu_C \equiv 0, 8 \,(\mathrm{mod}\, 16) : R_\epsilon^{em} = e^{i\pi\nu_C/8},\ R_\epsilon^{me} = -e^{i\pi\nu_C/8},\\
&\nu_C \equiv \pm 4 \,(\mathrm{mod}\, 16) : R_\epsilon^{em} = R_\epsilon^{me} = 1,\\
&\nu_C \equiv \pm 2 \,(\mathrm{mod}\, 4) : R_\epsilon^{a\bar{a}} = R_\epsilon^{\bar{a}a} = e^{-i\pi\nu_C/8}.
\end{aligned} \tag{46}$$

For all three cases, the phase, accumulated on a full circle, is

$$R_c^{\sigma_1\sigma_2} R_c^{\sigma_2\sigma_1} = e^{i(\pi+\pi\nu_C/4)}, \tag{47}$$

which agrees with the phase from Eq. (45). Thus, we have verified that all topological spins, fusion rules, and phases are consistent with Ref. [15]. Furthermore, the results in Eqs. (32), (33), (42), and (45) are invariant under the change of $\nu_C \to \nu_C \pm 16$. Therefore, we conclude that the Abelian topological orders in Fig. 2 agree with Kitaev's sixteenfold way.

B. Sixteenfold way for non-Abelian topological orders

The non-Abelian topological orders introduced in Sec. II can be viewed as direct products between an Ising conformal field theory and an Abelian U(1) sector. The Abelian sector is still described by the K matrix in Eq. (7). Here, we examine the extra contribution from the Ising CFT. To prevent confusion with the vortex σ, we change the notation for the spin field in the $e/4$-quasiparticle operator to χ. As a reminder, the fusion rules for χ are $\chi \times \psi = \chi$ and $\chi \times \chi = \psi + I$ [9]. Here, ψ is the Majorana field with the conformal dimension $\frac{1}{2}$. The phase induced from exchanging two χ is given by

$$\theta_I^{\chi\chi} = -\frac{\pi}{8}\mathrm{sgn}(\nu_C), \quad \theta_\psi^{\chi\chi} = \frac{3\pi}{8}\mathrm{sgn}(\nu_C). \tag{48}$$

Here, ν_C is the Chern number of the non-Abelian topological order which differs from Chern number of the associated U(1) Abelian sector by ± 1.

1. Topological spin

The neutral fermion ε is identified as

$$\varepsilon = \prod_{i=1}^{N} e^{in_i\phi_i} \quad \text{or} \quad \varepsilon = \psi \prod_{i=1}^{N} e^{im_i\phi_i}. \tag{49}$$

Here, $\sum n_i$ is odd, whereas $\sum m_i$ is even. From this definition, we automatically have $\theta_\varepsilon = -1$. The non-Abelian vortex is

$$\sigma = \chi \prod_{i=1}^{N} e^{i\left(\frac{1}{2}+l_i\right)\phi_i}. \tag{50}$$

Based on the above definition, one can easily verify that $\sigma \times \sigma = \varepsilon + I$ and $\sigma \times \varepsilon = \sigma$. These fusion rules are consistent with Table 1 in Ref. [15]. Although N only counts the modes of the U(1) Abelian sector, $\vartheta_\sigma = e^{i\pi\nu_C/8}$ is still satisfied since the conformal dimension of χ is $\frac{1}{16}$. This contributes an additional factor of $e^{i\pi\,\mathrm{sgn}(\nu_C)/8}$ to the topological spin.

2. Braiding rules

For the fermion in Eq. (49) and the vortex in Eq. (50), the phase induced by moving one of them around the other is

$$\begin{aligned}
&\phi_\sigma^{\sigma\varepsilon} = 2\pi\ \mathrm{sgn}(\nu_C) \sum_{i=1}^{N} n_i\left(\frac{1}{2}+l_i\right) (\mathrm{mod}\, 2\pi)\\
\text{or}\quad &\phi_\sigma^{\sigma\varepsilon} = \mathrm{sgn}(\nu_C)\left[2\pi \sum_{i=1}^{N} m_i\left(\frac{1}{2}+l_i\right) - \pi\right] (\mathrm{mod}\, 2\pi).
\end{aligned} \tag{51}$$

In the second case, the additional π phase comes from moving χ around ψ. In both cases, the results reduce to

$$\phi_\sigma^{\sigma\varepsilon} = \pi. \tag{52}$$

Finally, the phase accumulated by exchanging a pair of non-Abelian vortices can be decomposed into two parts:

$$\theta_\beta^{\sigma\sigma} = \theta_{\beta_1}^{\chi\chi} + \theta_{\beta_2}^{\sigma_A\sigma_A}. \tag{53}$$

In the above equation, σ_A represents the Abelian vortices obtained from σ by detaching χ. Also, β_1 and β_2 should fuse into β, where β, β_1, and β_2 can be either I or $\varepsilon = \psi$. Let us first assume that the two Abelian vortices σ_A are described by identical operators. It is then meaningful to ask about the phase, accumulated when their positions are exchanged.

We start with the scenario of $\nu_C > 0$. If $\nu_C \equiv 1 \,(\mathrm{mod}\, 4)$, then the two possible triplets for $(\beta, \beta_1, \beta_2)$ are (I, I, I) and $(\varepsilon, \psi = \varepsilon, I)$. Then, one has

$$\begin{aligned}
\theta_I^{\sigma\sigma} &= \theta_I^{\chi\chi} + \theta_I^{\sigma_A\sigma_A} = -\frac{\pi}{8} + \frac{\pi}{8}(\nu_C - 1) = \frac{\pi}{8}(\nu_C - 2),\\
\theta_\varepsilon^{\sigma\sigma} &= \theta_\psi^{\chi\chi} + \theta_I^{\sigma_A\sigma_A} = \frac{3\pi}{8} + \frac{\pi}{8}(\nu_C - 1) = \frac{\pi}{8}(\nu_C + 2).
\end{aligned} \tag{54}$$

When $\nu_C \equiv 3 \,(\mathrm{mod}\, 4)$, the two possible triplets for $(\beta, \beta_1, \beta_2)$ become (I, ψ, ε) and $(\varepsilon, I, \varepsilon)$. Thus,

$$\begin{aligned}
\theta_I^{\sigma\sigma} &= \theta_\psi^{\chi\chi} + \theta_\varepsilon^{\sigma_A\sigma_A} = \frac{3\pi}{8} + \frac{\pi}{8}(\nu_C - 1) = \frac{\pi}{8}(\nu_C + 2),\\
\theta_\varepsilon^{\sigma\sigma} &= \theta_I^{\chi\chi} + \theta_\varepsilon^{\sigma_A\sigma_A} = -\frac{\pi}{8} + \frac{\pi}{8}(\nu_C - 1) = \frac{\pi}{8}(\nu_C - 2).
\end{aligned} \tag{55}$$

Similarly, one can also calculate $\theta_I^{\sigma\sigma}$ and $\theta_\varepsilon^{\sigma\sigma}$ for negative ν_C. For all the four cases, the results can be rewritten as

$$\theta_I^{\sigma\sigma} = \frac{\pi}{8}\left(\nu_C^2 - \nu_C - 1\right) (\mathrm{mod}\, 2\pi), \tag{56}$$

$$\theta_\varepsilon^{\sigma\sigma} = \frac{\pi}{8}\left(\nu_C^2 + 3\nu_C - 1\right) (\mathrm{mod}\, 2\pi), \tag{57}$$

which agree with the braiding rules listed in Table 1 in Ref. [15]. For encircling one vortex around another vortex, one has

$$\phi_I^{\sigma\sigma} \equiv -\frac{\pi\nu_C}{4} (\mathrm{mod}\, 2\pi), \tag{58}$$

$$\phi_\varepsilon^{\sigma\sigma} \equiv \frac{3\pi\nu_C}{4} (\mathrm{mod}\, 2\pi). \tag{59}$$

To finish our discussion, we need to address the situation in which the Abelian parts σ_A of the two vortices differ. Since we no longer consider identical operators for the two excitations,

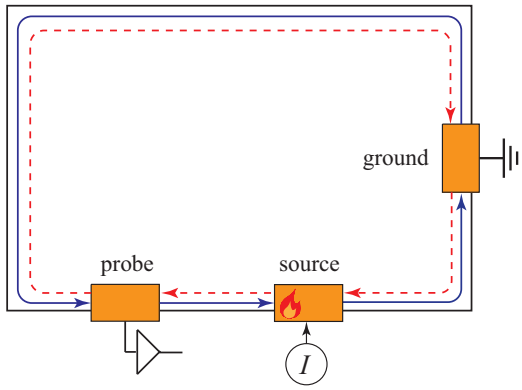

FIG. 3. Dashed lines show upstream neutral modes. Solid lines show the charged mode. The neutral mode is excited at the hot spot in the source.

it is only meaningful to ask about the phase, accumulated when one anyon makes a complete circle around the other. The results turn out the same as in the above equations (58) and (59).

To conclude, we have demonstrated that the sixteenfold way is satisfied for all the topological orders introduced in Sec. II. This important feature will be useful when we discuss interferometry in Sec. V.

IV. EXPERIMENTAL SIGNATURES

A. Upstream modes

The simplest experimental signature is the presence or absence of upstream neutral modes. It can be tested by probing upstream noise in the setup [70] of Fig. 3. The source in Fig. 3 is maintained at a finite voltage, while the chiral charged mode enters it at zero voltage. Thus, a nonequilibrium hot spot [124–126] forms at the point where the chiral charged mode enters the contact. Energy, dissipated in the hot spot, is carried by the upstream neutral mode toward the probe and heats it. This results in excess noise in the probe. Other related setups [67,68] were also proposed and used to observe upstream neutral modes.

Clearly, energy can only go upstream in the states with the negative Chern number ν_C. A subtlety involves a possibility of upstream energy transport due to edge reconstruction [61], if the edge is not long enough. This issue has been tackled experimentally by comparing the upstream noise at $\nu = \frac{5}{2}$ in GaAs with the upstream noise at $\nu = \frac{7}{3}$ and $\frac{8}{3}$ [68]. There is a topologically protected upstream mode at $\nu = \frac{8}{3}$ but not at $\nu = \frac{7}{3}$ (see Ref. [65] for a review of the $\frac{8}{3}$ and $\frac{7}{3}$ states in GaAs). Thus, if, in a given device, upstream noise is seen at $\nu = \frac{8}{3}$ but not at $\nu = \frac{7}{3}$, then the device can probe topologically protected upstream transport at other close filling factors.

B. Thermal Hall conductance

The thermal Hall conductance provides a complementary probe of the neutral modes. The existing thermal transport experiments cannot tell upstream modes from downstream modes [62,127] since the experiments cannot determine the sign of the thermal conductance coefficient. Hence, to find the Chern number, one also has to test the presence of upstream modes. Thus, the thermal transport approach is most powerful if combined with the approach from the previous subsection.

In this type of experiment, the Hall bar is connected with two heat reservoirs at different temperatures. One defines the thermal Hall conductance as $g_Q = dJ_Q/dT = \kappa T$ where κ is the thermal conductance coefficient and J_Q is the heat current. In an FQH system, the thermal energy is mainly carried by the edge modes. These edge modes are essentially one-dimensional ballistic channels. In the limit of a long propagation length, it was shown that $\kappa = c\kappa_0$, where $\kappa_0 = \pi^2 k_B^2/(3h)$ and c denotes the central charge of the topological order which is related to the net number of the downstream modes [14,63,64]. A negative c corresponds to upstream heat transport.

For the $\nu = \frac{5}{2}$ FQH system, there are two downstream bosonic modes from the filled lowest Landau level. Also, an additional downstream charged bosonic mode exists for the second Landau level with $\nu = \frac{1}{2}$. Finally, each topological order has its unique neutral sector. In other words, the central charges for different topological orders are different. For Abelian orders, all neutral modes are bosonic. Each contributes ± 1 to the central charge, depending on the propagation direction. Hence, the thermal conductance coefficient is given by

$$\kappa = (2 + 1 \pm N)\frac{\pi^2 k_B^2}{3h} = (3 \pm N)\frac{\pi^2 k_B^2}{3h}, \tag{60}$$

where the minus sign corresponds to upstream neutral modes. On the other hand, a single Majorana mode exists at the edge of a non-Abelian system. The central charge of the Majorana mode is $\pm\frac{1}{2}$. Therefore, one has

$$\kappa = \left[3 \pm \left(N + \frac{1}{2}\right)\right]\frac{\pi^2 k_B^2}{3h}. \tag{61}$$

The positive (negative) sign corresponds to topological orders with downstream (upstream) neutral modes. Recently, the thermal conductance of $\kappa = 2.5\kappa_0$ was reported in a $\nu = \frac{5}{2}$ FQH system in GaAs [62] in agreement with the predictions [24] for the PH-Pfaffian state. Equations (60) and (61) apply to long edges in thermal equilibrium. See Refs. [62,65,127,128] for a discussion of finite-size effects in some of the states.

C. Tunneling

A very different approach to probe topological order is tunneling transport [35–37,54]. Imagine that a constriction is created in an FQH liquid (Fig. 4). Quasiparticles can then tunnel through the constriction. To estimate the tunneling conductance, one uses the scaling dimensions (21) and (25) of the quasiparticle operators Δ_q, where q stands for the quasiparticle type. At low temperatures, the linear conductance can be found from the renormalization group (RG) and is determined by the scaling dimension of the most relevant tunneling operator $\Gamma\Psi_{qu}^\dagger\Psi_{qd}$, where $\Psi_{qu,qd}$ denote the quasiparticle operators on the upper and lower edges on the two sides of the constriction QPC. Under the action of RG, Γ grows as $E^{2\Delta_q - 1}$, where E is the energy cutoff. Thus, $\Gamma_{\rm eff}(T) \sim T^{2\Delta_q - 1}$ at the energy scale set by the temperature. The conductance $G \sim |\Gamma_{\rm eff}(T)|^2 \sim T^{4\Delta_q - 2} = T^{2g-2}$ [60].

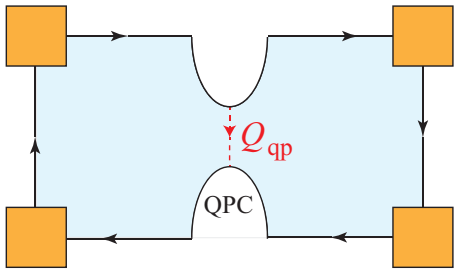

FIG. 4. Quasiparticle tunneling in the quantum point contact (QPC) is shown by the dashed line.

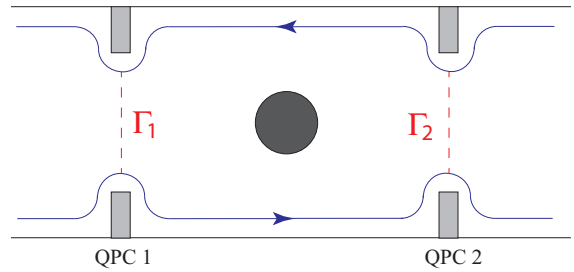

FIG. 5. A Fabry-Pérot interferometer with two quantum point contacts. Quasiparticles traveling along the edge tunnel at the two contacts with the amplitudes Γ_1 and Γ_2. The number of the quasiparticles in the antidot (dark circle in the middle) is controlled by the gate voltage.

The tunneling exponents g are listed in Table VI. The most relevant quasiparticle is the $e/2$ particle in most states, and hence $g = \frac{1}{2}$ for a majority of the states. Smaller values of g correspond to $\nu_C = 0,\ \pm1$, and ±2, that is, the $K = 8$, Pfaffian, PH-Pfaffian, 331, and 113 states. We generally expect that the tunneling amplitudes $\Gamma_{1,2}$ are higher for lower-charge particles. Thus, *unrenormalized* tunneling amplitudes are expected to be higher for $e/4$ quasiparticles than for $e/2$ quasiparticles. The dominant low-energy tunneling process depends on the renormalized amplitudes. At $|\nu_C| < 3$, the most relevant tunneling operator is that of $e/4$ particles and hence they dominate tunneling. At $\nu_C = \pm3$, the $e/4$- and $e/2$-tunneling operators have the same scaling dimension, so it is plausible that the $e/4$ tunneling dominates. On the other hand, at $|\nu_C| \geqslant 7$, the $e/4$-tunneling operator is marginal or irrelevant. Hence, the $e/2$ tunneling is more important. The case of $3 < |\nu_C| < 7$ is subtle. Both the $e/4$ and $e/2$ tunneling are relevant in the RG sense, yet, the $e/2$-tunneling operator has a lower scaling dimension. What sort of particles dominate depends then on the ratio of their unrenormalized tunneling amplitudes.

The above discussion tacitly assumed that the neutral modes do not interact with the charged mode. As we explain below, the results for the tunneling exponents do not depend on this assumption. This point is well known for positive Chern numbers [60]. For negative Chern numbers and in the absence of disorder, the exponents are nonuniversal [60]. The PH-Pfaffian state ($\nu_C = -1$) is an exception to this rule since no RG-relevant interaction between a single upstream Majorana mode and the charged mode exists in that case [24]. For $\nu_C < -2$, the universality of the tunneling exponents is guaranteed by disorder [25,34,38]. Thus, only the 113 state with $\nu_C = -2$ should show a dependence of tunneling exponents on the interaction of the upstream neutral and downstream charged modes. Even in that case, the interaction effect is weak [39] and will be neglected below.

The predicted scaling is only observed in the absence of Coulomb interaction across the constriction [38,129], edge reconstruction [130,131], and dissipation [132]. Otherwise, one expects a nonuniversal g that exceeds the ideal theoretical value. In a very clean sample, momentum-resolved tunneling [133,134] would give detailed information about the structure of the edge.

D. Fabry-Pérot interferometry

In order to directly probe the fractional statistics of anyons in the fractional quantum Hall system, it is necessary to braid quasiparticles and examine the consequences. An experimental technique based on a Fabry-Pérot interferometer was proposed by Chamon *et al.* for Abelian states [80]. Later, the same technique was generalized to study $\nu = \frac{5}{2}$ fractional quantum Hall systems [9,72,73] and many other FQH states [82–87]. In this section, we review Fabry-Pérot interferometry for all states introduced in Sec. II. The key feature is the topological even-odd effect [72,73] which was originally predicted for the Pfaffian state, but can easily be seen to occur in all non-Abelian states. Depending on the details, it can also be mimicked by Abelian orders [88].

In Fig. 5, we sketch a Fabry-Pérot interferometer with two quantum point contacts (QPC). Quasiparticles traveling along an edge can tunnel to the opposite edge at the contacts, with the corresponding tunneling amplitudes Γ_1 and Γ_2. These values are controlled by tuning the voltage on the gates that define the QPCs. In the middle of the interferometer, an antidot is created by applying a voltage to the central gate. By tuning the voltage there, the number of quasiparticles in the antidot can be adjusted. In the experiment, an interference pattern in the tunneling current due to two possible tunneling paths is measured.

In the following discussion, we will only focus on the weak-tunneling regime. We assume that both Γ_1 and Γ_2 are small, such that the backscattering current between the upper and lower edges of the interferometer is determined by the single-particle tunneling probability. To the lowest order in Γ_1 and Γ_2, the tunneling probability is given by [9,73]

$$p = r[|\Gamma_1|^2 + |\Gamma_2|^2 + 2u|\Gamma_1||\Gamma_2|\cos(\phi_{\rm AB} + \phi_s + \delta)], \quad (62)$$

where $\phi_{\rm AB}$ denotes the Aharonov-Bohm phase and ϕ_s is the statistical phase, accumulated by a quasiparticle that makes a full circle around the interferometer. We define $\delta = \arg(\Gamma_2/\Gamma_1)$. $r = r(V,T)$ and $u = u(V,T)$ depend on microscopic details. They satisfy one important constraint. Indeed, the current must flow from higher voltage to lower voltage irrespective of the Aharonov-Bohm phase $\phi_{\rm AB}$. In other words, the current cannot change sign as a function of $\phi_{\rm AB}$. This means that the combination

$$s = \frac{2|u\Gamma_1\Gamma_2|}{|\Gamma_1|^2 + |\Gamma_2|^2} \quad (63)$$

must satisfy the inequality

$$s \leqslant 1. \tag{64}$$

1. Tunneling operators

Equation (62) tacitly assumes that only one type of quasiparticle is allowed to tunnel. This is never the case and the Hamiltonian of an interferometer assumes the form

$$H = H_{\text{edges}} + \sum_{\alpha} \left(\Gamma_1^{\alpha} T_1^{\alpha} + \Gamma_2^{\alpha} T_2^{\alpha} + \text{H.c.}\right), \tag{65}$$

where H_{edges} describes the edges [see Eqs. (18) and (22)]; $\Gamma_{1,2}^{\alpha}$ and $T_{1,2}^{\alpha}$ are the tunneling amplitudes and the tunneling operators for quasiparticle type α at QPC1 and QPC2. The index α covers both electric and topological charges.

We have argued in Sec. IV C that quasiparticles of only one electric charge can be expected to dominate tunneling. This charge is either $e/4$ or $e/2$. The $e/2$ case is easy since there is only one allowed most relevant tunneling operator $T = \exp(i[\phi_\rho^u - \phi_\rho^d]/2)$, where the indices u and d refer to the upper and lower edges. Thus, we come back to Eq. (62). The situation is more complex for $e/4$ particles, provided that $\nu_C \neq 0$.

One complication is a possibility that $e/4$ and $e/2$ particles dominate tunneling at the two different QPCs. To avoid that issue, we will assume that QPC1 and QPC2 are identical. In particular, $|\Gamma_1^{\alpha}| = |\Gamma_2^{\alpha}|$. This assumption will also be used in our discussion of Mach-Zehnder interferometry below. Second, in all Abelian orders with $\nu_C \neq 0$, there are two topologically distinct $e/4$ quasiparticles. Thus, two different tunneling operators must be included at each QPC. This will be of great importance in subsequent sections.

We observe that one tunneling operator is sufficient in Eq. (65) for $e/2$ tunneling in all states and for $e/4$ tunneling in all non-Abelian states and in the $K = 8$ state ($\nu_C = 0$). All other Abelian orders (integer $\nu_C \neq 0$) should be described by Hamiltonians that include tunneling of two sorts of $e/4$ quasiparticles.

One more subtlety involves a possibility of several equally relevant quasiparticle operators for $e/4$ particles. For example, at $\nu_C = 4$, such operators are $Q_+ = \exp(i\phi_\rho/2)\exp(i[\phi_1 + \phi_2]/2)$ and $Q_- = \exp(i\phi_\rho/2)\exp(-i[\phi_1 + \phi_2]/2)$. A tunneling operator T_i^{α} can include contributions from all such quasiparticle operators, consistent with label α. This point is of little consequence at $|\nu_C| \leqslant 2$, but affects possible values of s [Eqs. (63) and (64)] at $|\nu_C| > 2$. Naively, any value of $0 \leqslant s \leqslant 1$ is allowed and $s \to 1$ at $V, T \to 0$. The argument is based on the renormalization group treatment of the Hamiltonian (65). Indeed, the renormalization group procedure decreases the distance between any two points on each step. When the distance becomes shorter than the ultraviolet cutoff, the points can be seen as merging. Hence, if the thermal and voltage lengths $\hbar v_{\rho,n}/T$ and $\hbar v_{\rho,n}/eV$ exceed the interferometer size, the renormalization group procedure stops after the two tunneling contacts end up in the same spatial point. For identical T_1 and T_2, this implies $u(V, T) = 1$. Hence, $s = 1$ at $|\Gamma_1| = |\Gamma_2|$.

The above argument works, provided that the edge actions are given by equations of the type (18) and (22). A realistic system may well not be described by this type of an action even in the scaling limit, where all irrelevant operators can be ignored. Indeed, relevant perturbations are missing in our simplest equations for the edge actions. One such perturbation is present at any ν_C. It is the random potential that couples to the charged mode: $w(x)\partial_x\phi_\rho$. Such perturbation can be eliminated from the Hamiltonian density $\frac{v_\rho}{2\pi}(\partial_x\phi_\rho)^2 + w(x)\partial_x\phi_\rho$ by the variable shift $\phi_\rho \to \phi_\rho + \pi \int w(x)dx/v_\rho$. The shift changes the relative phases of Γ_1 and Γ_2 and has no effect on the range of s. Similar perturbations are among various relevant perturbations that involve neutral modes. For example, the perturbation $P_n = w_n(x)\partial_x\phi_1$ is allowed. Such perturbations do not affect the range of s at $|\nu_C| \leqslant 2$. This changes at $|\nu_C| > 2$. Indeed, P_n can be eliminated by a shift of ϕ_1. This changes the relative phases of the contributions, containing Q_1 and Q_2, in the tunneling operators. As a result, T_1 and T_2 cease being identical. This undermines the argument for the possibility to reach $s = 1$.

We now turn to the analysis of the current through the interferometer. First, we consider the situation, in which the tunneling process is dominated by the $e/4$ quasiparticles.

2. Non-Abelian topological orders

Suppose an $e/4$ quasiparticle is sent to the interferometer as a probe particle. The braiding phase it accumulates around the antidot is given by

$$\phi_s = \frac{n\pi}{4} + \phi_\beta^{\sigma\alpha}. \tag{66}$$

Here, $ne/4$ is the total charge inside the interferometer (i.e., n is the number of $e/4$ quasiparticles), α denotes the topological charge inside the interferometer, and β is the fusion outcome between σ and α. The phase $\phi_\beta^{\sigma\alpha}$ comes from the neutral degrees of freedom. The first term $n\pi/4$ comes from the Abelian charged sector which is the same in all 16 states. As a reminder, we quote the results for $\phi_\beta^{\sigma\alpha}$ from Sec. III:

$$\phi_I^{\sigma\sigma} \equiv -\frac{\pi\nu_C}{4} \pmod{2\pi}, \tag{67}$$

$$\phi_\psi^{\sigma\sigma} \equiv \frac{3\pi\nu_C}{4} \pmod{2\pi}, \tag{68}$$

$$\phi_\sigma^{\sigma\psi} = \pi \tag{69}$$

$$\phi_\sigma^{\sigma I} = 0. \tag{70}$$

When the number n of trapped quasiparticles is odd, then $\alpha = \sigma$. Since $\sigma \times \sigma = \psi + I$, there are two possible fusion channels for the vortices. Both channels contribute to the measured backscattering current. Moreover, the probabilities of having $\beta = \psi$ and I are the same. From Eqs. (58) and (59), the phase difference between the two cases is determined as

$$\Delta\phi = \phi_\psi^{\sigma\sigma} - \phi_I^{\sigma\sigma} = \frac{3\pi\nu_C}{4} - \left(-\frac{\pi\nu_C}{4}\right) \equiv \pi \pmod{2\pi}. \tag{71}$$

Therefore, the two fusion channels correspond to the opposite values of the cosine term in the probability (62). Hence, the tunneling current does not depend on the magnetic flux enclosed by the two QPCs.

On the other hand, α can be either I or ψ when n is even. Nevertheless, the antidot must be in one of the superselection

states, but not in their superposition. In Sec. III, we found that $\phi_\sigma^{\sigma\psi} = \pi$ and $\phi_\sigma^{\sigma I} = 0$ (the second equation is, of course, trivial). Furthermore, these two values are independent of ν_C. Therefore, we conclude that for all non-Abelian topological orders satisfying the sixteenfold way, the flux-dependent term in the tunneling current is given by

$$n \text{ is odd} : I_\Phi = 0, \tag{72}$$

$$n \text{ is even} : I_\Phi = \frac{er}{2}|\Gamma_1||\Gamma_2| \cos\left(\gamma + \frac{n\pi}{4} + N_\psi \pi\right). \tag{73}$$

Here, $N_\psi = 1$ if the antidot has the topological charge ψ, $N_\psi = 0$ otherwise. Also, we have defined $\gamma = \phi_{\rm AB} + \delta$. The above expresses the celebrated even-odd effect.

3. Abelian topological orders with flavor symmetry

It has been argued that the even-odd effect was observed experimentally at $\nu = \frac{5}{2}$ [50,52]. At this time, the interpretation of the experiment remains ambiguous [135], in part, because the even-odd effect may also be observed [88] in the Abelian 331 state. Below, we argue that all the Abelian orders in the sixteenfold way can demonstrate the same effect if they have the exact flavor symmetry for the two species of quasiparticles σ_1 and σ_2. The $K = 8$ order is an exception since it has only one quasiparticle type. The flavor symmetry is defined as the equivalence of the two quasiparticle types. This implies two properties: (i) the two species of quasiparticles have the same tunneling amplitudes at the QPC; and (ii) the probabilities of their presence in the antidot are the same. For us, only (i) matters.

Suppose the antidot contains a total number of n quasiparticles, such that n_1 of them are the first species of vortex and n_2 of them are the second species of vortex. Then, the condition $n = n_1 + n_2$ must hold. Due to the exact flavor symmetry, the topological charge of the probe particle can be either σ_1 or σ_2 with the same probability. Depending on the species of the probe particle, the phase from encircling the antidot is given by

$$\phi_1 = \frac{n\pi}{4} + n_1\phi_{c_1}^{\sigma_1\sigma_1} + n_2\phi_{c_2}^{\sigma_1\sigma_2}, \tag{74}$$

$$\phi_2 = \frac{n\pi}{4} + n_1\phi_{c_2}^{\sigma_2\sigma_1} + n_2\phi_{c_1}^{\sigma_2\sigma_2}. \tag{75}$$

In Sec. III, we proved that $\phi_{c_1}^{\sigma_1\sigma_1} = \phi_{c_1}^{\sigma_2\sigma_2} = \pi\nu_C/4$ and $\phi_{c_2}^{\sigma_1\sigma_2} = \phi_{c_2}^{\sigma_2\sigma_1} = \pi\nu_C/4 + \pi$. Thus, we obtain

$$\phi_1 = \frac{n\pi}{4} + (n_1 + n_2)\frac{\pi\nu_C}{4} + n_2\pi, \tag{76}$$

$$\phi_2 = \frac{n\pi}{4} + (n_1 + n_2)\frac{\pi\nu_C}{4} + n_1\pi. \tag{77}$$

The phase difference between the two cases is given by $\Delta\phi = \phi_1 - \phi_2 = (n_2 - n_1)\pi$. When n is odd, $\Delta\phi \equiv \pi \pmod{2\pi}$ which implies that the measured backscattering current would have no oscillating pattern. On the other hand, $\Delta\phi \equiv 0 \pmod{2\pi}$ when n is even. Hence, constructive interference is present. Now, the evenness of n means that n_1 and n_2 can be either both even or both odd. From Eqs. (76) and (77), we see that a change in the parity of n_1 and n_2 shifts both ϕ_1 and ϕ_2 by a phase of π. This phenomenon is identical to the result for non-Abelian topological orders where two different topological charges of the antidot are possible at each even n, and correspond to two phases that differ by π. Therefore, we conclude that all topological orders satisfying the sixteenfold way can demonstrate the even-odd effect if the Abelian orders have an exact symmetry for the $e/4$ quasiparticles.

4. e/2-quasiparticle tunneling

We complete our discussion of Fabry-Pérot interferometery by examining the tunneling current when the tunneling process is dominated by the $(e/2, I)$ quasiparticles. In this scenario, the braiding phase from moving an $(e/2, I)$ quasiparticle around an $e/4$ particle is $\pi n/2$. Hence, the periodic term for the backscattering current is given by [85]

$$I_{e/2} \propto \cos\left(\frac{2\pi\Phi}{2\Phi_0} + \frac{n\pi}{2}\right), \tag{78}$$

where $\Phi_0 = hc/e$ and Φ is the magnetic flux. In other words, the backscattering current can tell nothing about the nature of the topological order.

V. MACH-ZEHNDER INTERFEROMETRY

In this section, we consider a more complicated setup than a Fabry-Pérot interferometer. A Mach-Zehnder interferometer [89,95] is harder to fabricate, but it offers two advantages over other approaches to interferometry. First, it produces substantially different signatures for different topological orders of the sixteenfold way. Second, this approach is immune to complications from fluctuations of the quasiparticle charge inside the interferometer [90]. If such fluctuations happen on a shorter timescale than a typical time interval between tunneling events at the point contacts in the interferometer, then the fluctuations would destroy or greatly modify the interference picture in any device. Slow fluctuations still greatly affect the behavior of a Fabry-Pérot interferometer [91], while a Mach-Zehnder device is not sensitive to them.

The physics of a Mach-Zehnder interferometer is considerably more involved than in the experimental setups from the previous section. It was addressed for some topological orders before [24,74–79,89,93]. Our present goal is to review the expected signatures in all states of the sixteenfold way. We will consider not only the tunneling current, but also the low-frequency noise in the interferometer. At weak tunneling, the noise and the current are not independent probes in the Fabry-Pérot setup. Indeed, at $T = 0$, the noise $S = \int dt \langle I(0)I(t) + I(t)I(0)\rangle$ reduces to the Schottky formula $S = 2qI$, where q is the charge of tunneling quasiparticles [75]. Interestingly, the noise exhibits a much more complicated behavior in the Mach-Zehnder setup. This happens due to the memory of the previous tunneling events.

Below, we focus on zero temperature, so that quasiparticles can only tunnel from the edge with the higher electrochemical potential (edge 1) to the edge with the lower electrochemical potential (edge 2). A systematic treatment for systems at a finite temperature [75,136] can be found in Appendix.

A typical setup for a Mach-Zehnder interferometer is illustrated in Fig. 6. In the figure, the arrows show the propagation of charged modes along the quantum Hall edges. Quasiparticles are allowed to tunnel between the edges at the two quantum point contacts QPC1 and QPC2. Source S1 is biased

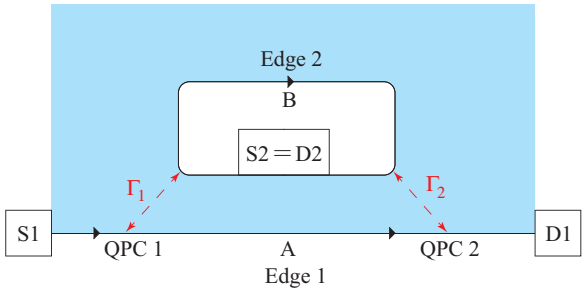

FIG. 6. A schematic picture of an electronic Mach-Zehnder interferometer. Charges propagate from source S1 to drain D1 and source S2 to drain D2. Tunneling is possible at the two quantum point contacts QPC1 and QPC2.

so that the electrochemical potential of edge 1 is higher than that of edge 2 by eV. We are interested in the tunneling current from source S1 to drain D2 and the corresponding noise, which depends on V and the magnetic flux enclosed by the loop QPC1-A-QPC2-B-QPC1.

The key piece of physics is the memory effect. Each quasiparticle, absorbed by drain D2, remains forever inside the loop QPC1-A-QPC2-B-QPC1. The probability of each subsequent tunneling event is affected by the mutual statistical phase ϕ_s of the tunneling quasiparticle and drain D2.

A. Tunneling current for non-Abelian orders

Since the bulk excitations are gapped, the system can be described by a low-energy edge theory. The tunneling process in Fig. 6 is modeled by the following Hamiltonian:

$$\hat{H} = \hat{H}_{\text{edge}} + [(\Gamma_1 \hat{T}_1 + \Gamma_2 \hat{T}_2) + \text{H.c.}], \tag{79}$$

where $\hat{H}_{\text{edge}}$ is the Hamiltonian for the two edges of the FQH liquid. The tunneling amplitudes for particles at the two quantum point contacts are labeled as Γ_1 and Γ_2, with the corresponding tunneling operators denoted as $\hat{T}_1$ and $\hat{T}_2$. Here, we choose a gauge such that both the Aharonov-Bohm phase ϕ_{AB} and the statistical phase ϕ_s are absorbed in $\hat{T}_2$. Depending on the number of neutral bosonic modes on the edge and the tunneling amplitudes for different types of quasiparticles, the tunneling process can be dominated by either $e/2$ or $e/4$ quasiparticles [see Eqs. (21) and (25)]. In the following, we will calculate the tunneling current for each case separately.

1. Case 1: e/4-quasiparticle tunneling

For all proposed non-Abelian topological orders in Sec. II, the fundamental excitations are quasiparticles with charge $e/4$. Suppose the tunneling process is dominated by $e/4$ quasiparticles. Then, there are six possible superselection sectors for drain D2 as shown in Fig. 7. Each sector is labeled by the electric and topological charges in parentheses. The electric charge is always $ne/4$, where $n = -1, 0, 1, 2$, since changing n by 4 amounts to adding the charge of a topologically trivial electron. Thus, $(-e/4, \sigma)$ can be considered to be in the same sector as $(3e/4, \sigma)$ [137]. Since the temperature is assumed to be zero, all transitions between different sectors are unidirectional.

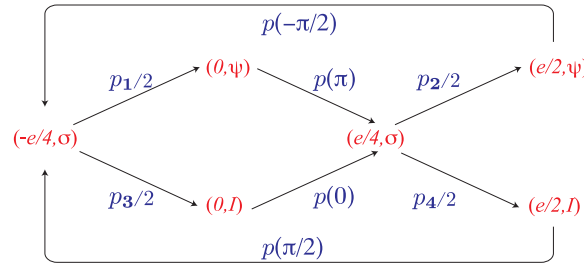

FIG. 7. The six possible superselection sectors for drain D2 when the tunneling is dominated by charge-$e/4$ quasiparticles. The arrows show all possible transitions between different sectors at zero temperature. The corresponding transition probabilities and statistical phases are shown in blue (four phases are listed in Table I).

When both Γ_1 and Γ_2 are small, and assuming that the fusion channel of the tunneling particle with the topological charge in D2 is known, a general expression for the transition rate between two sectors can be written as [89]

$$p(\phi_s) = r[(|\Gamma_1|^2 + |\Gamma_2|^2) + 2u|\Gamma_1||\Gamma_2|\cos(\phi_{\text{AB}} + \phi_s + \delta)], \tag{80}$$

with $\delta = \arg(\Gamma_2/\Gamma_1)$ and $u \leqslant 1$. Here, $\phi_{\text{AB}} = 2\pi\Phi/(4\Phi_0)$ is the Aharonov-Bohm phase accumulated by an $e/4$ quasiparticle moving around the interferometer loop QPC1-A-QPC2-B-QPC1. Four probabilities $p(n\pi/2)$ in Fig. 7 are given by the above expression with $\phi_s = n\pi/2$. The remaining probabilities are $p_{\mathbf{i}}/2$, where $p_{\mathbf{i}}$ is given by Eq. (80) with ϕ_s from Table I. The factor of $\frac{1}{2}$ in each probability comes from two possible fusion channels, $\sigma \times \sigma = I$ or ψ, and reflects the equal probabilities of the two fusion outcomes.

As shown in Fig. 7, there are four possible ways for drain D2 to absorb one electron charge from source S1 and return back to the original sector $(-e/4, \sigma)$. They correspond to four paths $\mathcal{P}_i$, $i = 1, \ldots, 4$, on the oriented graph in the figure. For example, one path $\mathcal{P}_1$ is $(-e/4, \sigma) \to (0, \psi) \to (e/4, \sigma) \to (e/2, \psi) \to (-e/4, \sigma)$. To compute the average current detected in drain D2, we need to know the average time $\bar{t}_{e/4}$ to transfer four successive quasiparticles: $I = e/\bar{t}_{e/4}$. The average time is a weighted sum of the average times $\bar{t}_{\mathcal{P}_i}$ to travel along each of the paths $\mathcal{P}_i$. For example, the probability q_1 that the system chooses path $\mathcal{P}_1$ equals

$$q_1 = \left(\frac{p_{\mathbf{1}}}{p_{\mathbf{1}} + p_{\mathbf{3}}}\right)\left(\frac{p_{\mathbf{2}}}{p_{\mathbf{2}} + p_{\mathbf{4}}}\right). \tag{81}$$

The average time is given by

$$\bar{t}_{e/4} = \sum_{i=1}^{4} q_i \bar{t}_{\mathcal{P}_i}, \tag{82}$$

where q_i are the probabilities of the four paths.

TABLE I. Statistical phases ϕ_s for transitions between different superselection sectors as shown in Fig. 7. Notice that $p_{\mathbf{1}} + p_{\mathbf{3}} = p_{\mathbf{2}} + p_{\mathbf{4}} = 2r(|\Gamma_1|^2 + |\Gamma_2|^2)$.

Index	ϕ_s	Index	ϕ_s
1	$\pi(3\nu_C - 1)/4$	**2**	$\pi(3\nu_C + 1)/4$
3	$-\pi(\nu_C + 1)/4$	**4**	$-\pi(\nu_C - 1)/4$

The expressions for q_i and $\mathcal{P}_i$ are similar for all i. We only show the contribution from the first path:

$$q_1\bar{t}_{\mathcal{P}_1} = \int_0^\infty \left[e^{-(p_1+p_3)t_1/2}\left(\frac{p_1}{2}\right)\right][e^{-p(\pi)t_2}p(\pi)] \times \left[e^{-(p_2+p_4)t_3/2}\left(\frac{p_2}{2}\right)\right]\left[e^{-p(-\frac{\pi}{2})t_4}p\left(-\frac{\pi}{2}\right)\right] \times (t_1+t_2+t_3+t_4)\,dt_1dt_2dt_3dt_4, \quad (83)$$

so that

$$\bar{t}_{\mathcal{P}_1} = \frac{2}{p_1+p_3} + \frac{1}{p(\pi)} + \frac{2}{p_2+p_4} + \frac{1}{p(-\pi/2)}. \quad (84)$$

For convenience in the later discussion, we define

$$A = \left(4 + \sum_{j=1}^{4} \frac{p_j}{p[(j+1)\pi/2]}\right). \quad (85)$$

After summing over all four paths with the weights q_i, we have

$$\bar{t}_{e/4} = \frac{A}{2r(|\Gamma_1|^2+|\Gamma_2|^2)}. \quad (86)$$

The same result can also be derived with the kinetic equation approach [75,89].

The tunneling current $I_{e/4} = e/\bar{t}_{e/4}$ takes four different values for different ν_C. Indeed, ϕ_s in Table I is invariant under $\nu_C \to \nu_C + 8$, and ν_C is an odd number for non-Abelian orders. In terms of the parameter $s = 2u|\Gamma_1||\Gamma_2|/(|\Gamma_1|^2 + |\Gamma_2|^2)$, Eqs. (63) and (64), one has

$$\text{when } \nu_C = 1: \quad I_{e/4} = \frac{er}{4}(|\Gamma_1|^2+|\Gamma_2|^2)\left[\frac{1-s^2+\frac{s^4}{4}\sin^2 2\gamma}{1-\frac{3s^2}{4}+\frac{s^4}{16}(1-\cos 4\gamma-\sin 4\gamma)}\right], \quad (87)$$

$$\text{when } \nu_C = -1: \quad I_{e/4} = \frac{er}{4}(|\Gamma_1|^2+|\Gamma_2|^2), \quad (88)$$

$$\text{when } \nu_C = 3 \text{ or } -5: \quad I_{e/4} = \frac{er}{4}(|\Gamma_1|^2+|\Gamma_2|^2)\left[\frac{1-s^2+\frac{s^4}{4}\sin^2 2\gamma}{1-\frac{s^2}{2}}\right], \quad (89)$$

$$\text{when } \nu_C = 5 \text{ or } -3: \quad I_{e/4} = \frac{er}{4}(|\Gamma_1|^2+|\Gamma_2|^2)\left[\frac{1-s^2+\frac{s^4}{4}\sin^2 2\gamma}{1-\frac{3s^2}{4}+\frac{s^4}{16}(1-\cos 4\gamma+\sin 4\gamma)}\right]. \quad (90)$$

In the above equations, we have defined $\gamma = \phi_{\rm AB} + \delta$. We remark that Eqs. (87) and (88) reproduce the results for the Pfaffian order [74] and the PH-Pfaffian order [24], respectively. The PH-Pfaffian case is strikingly different from all others since the current (88) exhibits no flux dependence. $\nu_C = \pm 7$ are not included in the above equations since $e/4$ particles are not expected to dominate tunneling at those Chern numbers.

2. Case 2: $e/2$-quasiparticle tunneling

As discussed in Sec. IV C, $e/4$ particles dominate tunneling at $|\nu_C| < 4$. At $|\nu_C| \geqslant 7$, the most important tunneling process involves $e/2$ particles. Both quasiparticle types can dominate tunneling at the intermediate values of the Chern number. Thus, it is essential to address the interference of both $e/4$ and $e/2$ charges. Below, we investigate the tunneling of the particles from the $(e/2, I)$ sector. In a striking contrast with the $e/4$ case, the results do not depend on statistics, at least, in the simplest model. In fact, the tunneling current is the same for the Abelian and non-Abelian orders.

As before, we denote the number of $e/4$ quasiparticles in D2 as n. Depending on the parity of n, possible superselection sectors for the drain are shown in Fig. 8. From the figure, one sees that the tunneling current depends on the parity of n. The Aharonov-Bohm phase becomes $\phi'_{\rm AB} = 2\pi\Phi/(2\Phi_0)$. The statistical phase is $\phi'_s = n\pi/2$ irrespectively of ν_C.

When n is odd, the topological charge for the drain can be σ only. The average time required for D2 to absorb one electron is then given by $\bar{t}_{e/2} = 1/p(-\pi/2) + 1/p(\pi/2)$. On the other hand, the topological charge of D2 can be either I or ψ, when n is even. In both cases, the time for D2 to absorb an electron is $\bar{t}_{e/2} = 1/p(0) + 1/p(\pi)$. Therefore, we determine the tunneling current $I_{e/2} = e/\bar{t}_{e/2}$ as

$$I_{e/2} = \frac{er}{2}(|\Gamma_1|^2+|\Gamma_2|^2)(1-s^2\sin^2\gamma') \quad \text{for odd } n, \quad (91)$$

$$I_{e/2} = \frac{er}{2}(|\Gamma_1|^2+|\Gamma_2|^2)(1-s^2\cos^2\gamma') \quad \text{for even } n. \quad (92)$$

Here, $\gamma' = \phi'_{\rm AB} + \delta$ and s has a similar definition to the definition in Eqs. (87)–(90). This result resembles the even-odd effect in the Fabry-Pérot interferometry.

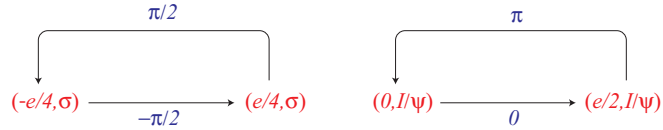

FIG. 8. Possible superselection sectors for drain D2 when the tunneling is dominated by charge-$e/2$ quasiparticles. The left (right) panel illustrates the scenario when the number of charge-$e/4$ quasiparticles in D2 is odd (even). When there are even number of quasiparticles in drain D2, the topological charge of the drain can be either I or ψ. However, the topological charge does not change after tunneling events since $e/2$ quasiparticles carry the trivial topological charge I. The arrows show all possible transitions between different sectors at zero temperature.

A more general analysis should incorporate rare tunneling events of charge-$e/4$ particles. Such tunneling events switch the system between the two sides of Fig. 8. In turn, the tunneling of $e/4$ particles is sensitive to possible tunneling of neutral fermions ψ. Fermion tunneling is marginal in the RG sense [113] and hence likely more important than the tunneling of $e/4$ charges at $|\nu_C| \geqslant 7$. To include such effects, it is necessary to set up a full set of kinetic equations. This cumbersome general procedure is beyond the scope of this paper. On the other hand, one does not need to include rare tunneling events of $e/2$ particles and neutral fermions in the analysis of the previous subsection, where we assumed that $e/4$ particles dominate. The difference between this subsection and the previous subsection is due to the fact that $e/4$-charge tunneling cycles the system through all superselection sectors. Any additional tunneling events just occasionally change the phase of the cycle. When the dominant tunneling process is due to $e/2$ particles, some superselection sectors are available only through rare tunneling events of other charges.

B. Fano factor in shot-noise experiment for non-Abelian orders

The Fano factor in a shot-noise experiment is another useful parameter to differentiate topological orders [75]. The nonequilibrium noise is defined as the Fourier transform of the current-current correlation function

$$S(\omega) = \frac{1}{2}\int_{-\infty}^{\infty} \langle \hat{I}(0)\hat{I}(t) + \hat{I}(t)\hat{I}(0)\rangle e^{i\omega t} dt. \tag{93}$$

This definition differs by a factor of $\frac{1}{2}$ from a definition, frequently found in the literature. We focus on the low-frequency limit. In this case, the shot noise can be written as $S = \overline{\delta Q^2(t)}/t$, where $Q(t)$ is the charge, transmitted through the interferometer over the time t, and $\delta Q(t)$ is its fluctuation. The Fano factor e^* is the ratio between the noise and the current:

$$e^* = S/I = \overline{\delta Q^2(t)}/Q(t) = e(\overline{\delta t^2}/\bar{t}^2), \tag{94}$$

where $\bar{t}$ is the average time needed to transfer the total charge e through the interferometer, and $\overline{\delta t^2}$ is the mean-square fluctuation of that time. The last equality in Eq. (94) was derived in Ref. [75].

We first assume that tunneling is dominated by $e/4$ particles. Now, we proceed to evaluate $\overline{t^2}_{e/4}$. One easily verifies that

$$\overline{t^2}_{e/4} = \sum q_i \overline{t^2}_{\mathcal{P}_i}, \tag{95}$$

where $\overline{t^2}_{\mathcal{P}_i}$ are the fluctuations of the times, corresponding to the four paths through the diagram in Fig. 7. For the path $\mathcal{P}_1$, the contribution $q_1\overline{t^2}_{\mathcal{P}_1}$ is given by

$$\begin{aligned}\int_0^\infty &\left[e^{-(p_1+p_3)t_1/2}\left(\frac{p_1}{2}\right)\right][e^{-p(\pi)t_2}p(\pi)]\\ &\times\left[e^{-(p_2+p_4)t_3/2}\left(\frac{p_2}{2}\right)\right]\left[e^{-p(-\frac{\pi}{2})t_4}p\left(-\frac{\pi}{2}\right)\right]\\ &\times(t_1+t_2+t_3+t_4)^2\,dt_1dt_2dt_3dt_4.\end{aligned} \tag{96}$$

This yields

$$\begin{aligned}\overline{t^2}_{\mathcal{P}_1} = &\frac{8}{(p_1+p_3)^2}+\frac{8}{(p_2+p_4)^2}+\frac{8}{(p_1+p_3)(p_2+p_4)}\\ &+\frac{4}{(p_1+p_3)p(\pi)}+\frac{4}{(p_1+p_3)p(-\pi/2)}\\ &+\frac{4}{(p_2+p_4)p(\pi)}+\frac{4}{(p_2+p_4)p(-\pi/2)}\\ &+\frac{2}{[p(\pi)]^2}+\frac{2}{[p(-\pi/2)]^2}+\frac{2}{p(\pi)p(-\pi/2)}.\end{aligned} \tag{97}$$

A lengthy but straightforward calculation for all four paths gives the following Fano factor:

$$\begin{aligned}\frac{e^*}{e} = &\frac{p_1p_3}{A^2}\left[\frac{1}{p(0)}-\frac{1}{p(\pi)}\right]^2+\frac{p_2p_4}{A^2}\left[\frac{1}{p(-\frac{\pi}{2})}-\frac{1}{p(\frac{\pi}{2})}\right]^2\\ &+\frac{p_1+p_3}{A^2}\sum_{j=1}^{4}\frac{p_j}{\{p[(j+1)\pi/2]\}^2}+\frac{8}{A^2}.\end{aligned} \tag{98}$$

By substituting the probabilities at different ν_C, one gets e^*/e as

$$\text{when } \nu_C = 1: \quad \frac{e^*}{e} = \frac{1}{4}\left[\frac{1-s^2+\frac{s^4}{4}(2+\cos 4\gamma-\sin 4\gamma)+\frac{s^6}{8}\sin 4\gamma-\frac{s^8}{128}(1-\cos 8\gamma)}{\left[1-\frac{3s^2}{4}+\frac{s^4}{16}(1-\cos 4\gamma-\sin 4\gamma)\right]^2}\right], \tag{99}$$

$$\text{when } \nu_C = -1: \quad \frac{e^*}{e} = \frac{1}{4}\left[\frac{1-\frac{s^2}{2}}{1-s^2+\frac{s^4}{8}(1-\cos 4\gamma)}\right], \tag{100}$$

$$\text{when } \nu_C = 3 \text{ or } -5: \quad \frac{e^*}{e} = \frac{1-\frac{s^2}{2}+\frac{s^4}{8}(1+3\cos 4\gamma)+\frac{s^6}{16}(1-\cos 4\gamma)}{(2-s^2)^2}, \tag{101}$$

$$\text{when } \nu_C = 5 \text{ or } -3: \quad \frac{e^*}{e} = \frac{1}{4}\left[\frac{1-s^2+\frac{s^4}{4}(2+\cos 4\gamma+\sin 4\gamma)-\frac{s^6}{8}\sin 4\gamma-\frac{s^8}{128}(1-\cos 8\gamma)}{\left[1-\frac{3s^2}{4}+\frac{s^4}{16}(1-\cos 4\gamma+\sin 4\gamma)\right]^2}\right]. \tag{102}$$

From these equations, we extract the maximal and minimal possible values of e^*/e in the limit of the maximal possible $s = 1$. Those values and the corresponding values of $\gamma = \phi_{AB} + \delta$ are summarized in Table II.

TABLE II. Maximal and minimal values of the Fano factor in a Mach-Zehnder interferometer experiment when $s = 1$. Here, we focus on non-Abelian orders for the $\nu = \frac{5}{2}$ FQH state and assume that the tunneling process is dominated by $e/4$ quasiparticles. The third and last columns provide the values for $\gamma = \phi_{AB} + \delta$ at which $e^* = e^*_{max}$ and $e^* = e^*_{min}$, respectively. Notice that these values of γ are modulo $\pi/2$.

ν_C (mod 8)	e^*_{max}/e	γ_{max}	e^*_{min}/e	γ_{min}
1	3.20	0.09	0.44	-0.82
3	1	0	3/8	$\pm\pi/4$
5	3.20	-0.09	0.44	0.82
7	∞	0	1/2	$\pm\pi/4$

When the tunneling process is dominated by $e/2$ quasiparticles, the physics is similar to that of a Laughlin state [75] as can be seen from Fig. 8. The Fano factor is simply given by

$$e^* = e\left[\frac{1 + s^2 \sin^2(\phi'_{AB} + \delta)}{2}\right], \tag{103}$$

or a similar expression with a cosine in place of the sine. Hence, the maximal value of the Fano factor is e in the limit of $\Gamma_1 \approx \Gamma_2$ and $u \approx 1$. The minimal Fano factor is always $e/2$.

C. Abelian topological orders with flavor symmetry

Similar calculations can be performed for Abelian topological orders. However, there are two different species of $e/4$ quasiparticles due to the two different types of vortices σ_1 and σ_2, as shown in Sec. III. Consequently, there are eight distinct superselection sectors for drain D2 as shown in Fig. 9. Generally, the two types of quasiparticles can have different tunneling amplitudes at the quantum point contacts. Thus, one has to consider many more transition rates than in the non-Abelian case. The calculations become very cumbersome. In the past, they were performed numerically for some of the proposed topological orders [78,79].

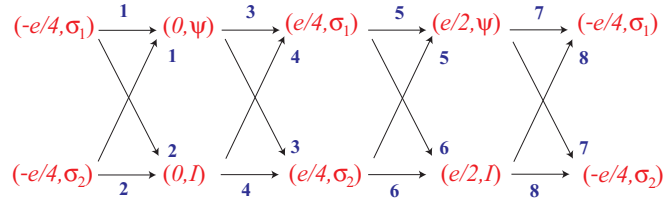

FIG. 9. For Abelian topological orders of the $\nu = \frac{5}{2}$ FQH state, there are eight superselection sectors for drain D2. The arrows show possible transitions between different sectors at zero temperature due to the tunneling of $e/4$ particles. The corresponding statistical phases are listed in Tables III and IV.

The statistical phase, accumulated after one $e/4$ quasiparticle encircles another, is still given by Eq. (66). Since the sixteenfold way is also satisfied by Abelian vortices, ϕ_s can be evaluated easily. Depending on the Chern number of the topological order, the results are shown in Tables III and IV.

In principle, the tunneling current and the Fano factor can be evaluated in essentially the same way as in the above subsection. To avoid unwieldy expressions, we focus on the situation with flavor symmetry of the quasiparticles. In other words, the tunneling amplitudes for the two types of $e/4$ quasiparticles at the QPCs are the same. Under this assumption, Fig. 9 reduces to a version of Fig. 7, as shown in Fig. 10. Using the same technique as before, we determine the tunneling current as

$$\text{when } \nu_C = 2 \text{ or } -6: \quad I_{e/4} = \frac{er}{2}\left[\frac{(|\Gamma_1|^2 + |\Gamma_2|^2)\left(1 - s^2 + \frac{s^4}{4}\sin^2 2\gamma\right)}{1 - \left(\frac{3}{4} - \frac{1}{4\sqrt{2}}\right)s^2 + \frac{s^4}{16}\left[\left(1 - \frac{1}{\sqrt{2}}\right)(1 - \cos 4\gamma) - \frac{1}{\sqrt{2}}\sin 4\gamma\right]}\right], \tag{104}$$

$$\text{when } \nu_C = 4 \text{ or } -4: \quad I_{e/4} = \frac{er}{2}\left[\frac{(|\Gamma_1|^2 + |\Gamma_2|^2)\left(1 - s^2 + \frac{s^4}{4}\sin^2 2\gamma\right)}{1 - \left(\frac{3}{4} - \frac{1}{4\sqrt{2}}\right)s^2 + \frac{s^4}{16}\left[\left(1 - \frac{1}{\sqrt{2}}\right)(1 - \cos 4\gamma) + \frac{1}{\sqrt{2}}\sin 4\gamma\right]}\right], \tag{105}$$

$$\text{when } \nu_C = 6 \text{ or } -2: \quad I_{e/4} = \frac{er}{2}\left[\frac{(|\Gamma_1|^2 + |\Gamma_2|^2)\left(1 - s^2 + \frac{s^4}{4}\sin^2 2\gamma\right)}{1 - \left(\frac{3}{4} + \frac{1}{4\sqrt{2}}\right)s^2 + \frac{s^4}{16}\left[\left(1 + \frac{1}{\sqrt{2}}\right)(1 - \cos 4\gamma) + \frac{1}{\sqrt{2}}\sin 4\gamma\right]}\right]. \tag{106}$$

Just as in the non-Abelian case, the results are grouped into four different classes (notice the sign differences in the denominator). It is easy to verify that the cases with $\nu_C = 2$ and -2 recover the expressions for the 331 order [78] and the 113 order [79], respectively. Finally, we remark that the tunneling current retains the structure of Eqs. (91) and (92), if the tunneling process is dominated by $e/2$ quasiparticles.

The Fano factor can be calculated in the same way as before. Since the expressions are too lengthy, we do not display them here. The maximal and minimal values of the Fano factors for different Chern numbers are found numerically and are summarized in Table V.

D. A special topological order: $K = 8$ state

In contrast to other Abelian orders, the $K = 8$ state is obtained by pairing two electrons into a charge-$2e$ boson. Then, the bosons condense into a Laughlin state with the filling factor of $\frac{1}{8}$ [115]. In this state, single-electron excitations are gapped. There are no neutral modes, and the vertex operator for the charge-$e/4$ quasiparticle is $e^{i\phi_\rho/2}$, where ϕ_ρ is the charged mode. In contrast to all other Abelian orders in the sixteenfold way, there is only one type of $e/4$ quasiparticle in the $K = 8$ state. Here, we examine its tunneling current and the Fano factor in a Mach-Zehnder experiment.

TABLE III. Statistical phase ϕ_s for the transitions between different superselection sectors as shown in Fig. 9. Here, $\nu_C \equiv 0 \pmod 4$.

Index	ϕ_s	Index	ϕ_s
1	$\pi(\nu_C+3)/4$	**5**	$\pi(\nu_C-3)/4$
2	$\pi(\nu_C-1)/4$	**6**	$\pi(\nu_C+1)/4$
3	π	**7**	$-\pi/2$
4	0	**8**	$\pi/2$

In Fig. 11, we show all eight possible superselection sectors for drain D2, with the corresponding transition probabilities. The phase accumulated by a quasiparticle, encircling the drain, equals $\phi_s = n\pi/4$, where the drain charge is $ne/4$ modulo $2e$, that is, $n = 0, 1, \ldots, 7$. In order for drain D2 to return to its initial superselection sector, it is necessary to transfer a total charge of $2e$. The structure of the diagram resembles the simple diagram of a Laughlin state [89].

From the figure, the average time required for eight successive tunneling events of charge-$e/4$ quasiparticles is given by $\bar{t} = \sum_{n=0}^{7} \frac{1}{p(n\pi/4)}$. The tunneling current is determined as $I = 2e/\bar{t}$. This leads to

$$I = \frac{er}{4}(|\Gamma_1|^2 + |\Gamma_2|^2)\left[\frac{1 - 2s^2 + \frac{5s^4}{4} - \frac{s^6}{4} + \frac{s^8}{64}\sin^2 4\gamma}{\left(1-\frac{s^2}{2}\right)\left(1 - s^2 + \frac{s^4}{8}\right)}\right]. \tag{107}$$

The variance of t can be evaluated as $\overline{\delta t^2} = \sum_{n=0}^{7}[1/p(n\pi/4)]^2$. This yields the following Fano factor:

$$\frac{e^*}{e} = \frac{64 - 160s^2 + 152s^4 - 68s^6 + \frac{29s^8}{2} - \frac{5s^{10}}{4} + \frac{s^{12}}{16} + \frac{s^{14}}{32}}{(2-s^2)^2(8-8s^2+s^4)^2} + \frac{s^8\left(\frac{7}{2} - \frac{15s^2}{4} + \frac{15s^4}{16} - \frac{s^6}{32}\right)}{(2-s^2)^2(8-8s^2+s^4)^2}\cos 8\gamma. \tag{108}$$

When $s = 1$, the Fano factor takes its maximum value $e^*_{\max} = 2e$ [78] at $\gamma = m\pi/4$. On the other hand, it assumes the minimum value $e^*_{\min}/e = 11/16$ at $\gamma = \pi/8 + m\pi/4$, where m is an integer. Equations (107) and (108) suggest that the tunneling current and the Fano factor are periodic in Φ with the period of $\Phi_0/2 = h/2e$. This agrees with the formation of Cooper pairs of electrons in the system [138].

VI. SUMMARY OF EXPERIMENTAL SIGNATURES

Experimental signatures of the topological orders of the sixteenfold way are summarized in Table VI. The PH-Pfaffian order seems to agree best with the existing data for the $\frac{5}{2}$ plateau in GaAs at the electron densities $n \sim 2$–3×10^{11} cm^{-2}. Indeed, this order possesses an upstream Majorana mode, has a tunneling exponent of $g_{e/4} = \frac{1}{4} < \frac{1}{2}$, demonstrates the even-odd effect in a Fabry-Pérot experiment, and shows the thermal Hall conductance coefficient of $\kappa_H = 2.5$, i.e., $\kappa = 2.5\kappa_0$.

TABLE IV. Statistical phase ϕ_s for the transitions between different superselection sectors as shown in Fig. 9. Here, $\nu_C \equiv 2 \pmod 4$.

Index	ϕ_s	Index	ϕ_s
1	$\pi(\nu_C-1)/4$	**5**	$\pi(\nu_C+1)/4$
2	$\pi(\nu_C+3)/4$	**6**	$\pi(\nu_C-3)/4$
3	π	**7**	$-\pi/2$
4	0	**8**	$\pi/2$

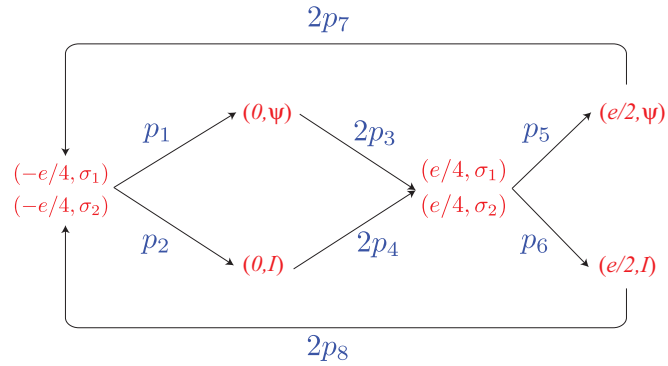

FIG. 10. Transitions between superselection sectors in an Abelian system with flavor symmetry. Note a coefficient of 2 in some of the probabilities. For example, the transition rate from the $(0, I)$ sector is $2p_4$ since this is the combined tunneling rate for two quasiparticle types.

VII. ITERATIVE COUPLED QUANTUM-HALL-STRIPES CONSTRUCTION

Effective Hamiltonians for different fractional quantum Hall states have been designed with coupled-wire constructions in Refs. [96–98,139,140]. Motivated by the mother-daughter relations from Sec. II, we propose an iterative construction of effective Hamiltonians for all orders in the sixteenfold way. In contrast to the previous work, we start with a collection of quantum Hall stripes and not wires (cf. Refs. [141–143]). We choose one of the 16 orders and assume that the ground state of the bulk Hamiltonian of each stripe has the chosen order. Such Hamiltonian is well known for the Pfaffian order [6,144]. Thus, we choose the Pfaffian order as our starting point in the following discussion. At the same time, all other orders can be used as a starting point.

We consider a large number of parallel stripes. The stripes host gapped QHE liquids in the bulk. In the absence of interaction between the stripes, they have gapless edge modes: charged and Majorana. We choose the interstripe interaction

TABLE V. Maximal and minimal values of the Fano factor in a Mach-Zehnder interferometer experiment when $s = 1$. Here, we focus on Abelian orders for the $\nu = \frac{5}{2}$ FQH state with flavor symmetry and assume that the tunneling process is dominated by $e/4$ quasiparticles. The third and last columns of the table show the values of $\gamma = \phi_{\rm AB} + \delta$ at which $e^* = e^*_{\max}$ and $e^*_{\min}$, respectively. Notice that these values are modulo $\pi/2$.

$\nu_C \pmod 8$	$e^*_{\max}/e$	$\gamma_{\max}$	$e^*_{\min}/e$	$\gamma_{\min}$
2	1.39	0.10	0.393	0.80
4	1.39	−0.10	0.393	−0.80
6	13.5	−0.05	0.381	0.98

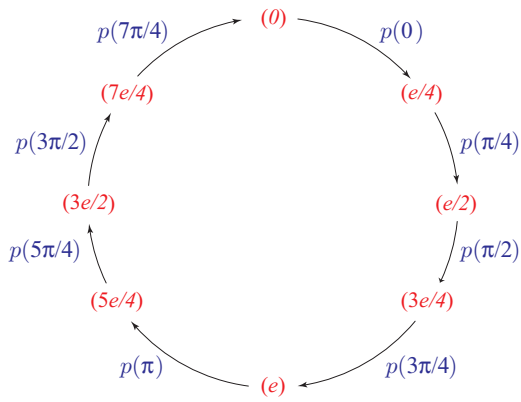

FIG. 11. In the $K = 8$ state, the superselection sectors of drain D2 are described by the drain's charge modulo $2e$. The drain makes a full circle through the diagram after eight tunneling events of $e/4$ quasiparticles.

that gaps those edge modes out. Indeed, our goal is to generate a system in which gapless edge modes are confined to its uppermost and downmost parts.

To demonstrate our idea, we start with constructing the effective Hamiltonian of the PH-Pfaffian state. This example provides a template for neutral-mode flipping in our coupled-stripe construction.

A. From Pfaffian to PH-Pfaffian

Consider a system of quantum Hall stripes in the Pfaffian state as illustrated in Fig. 12. First, assume no interstripe interaction. The Hamiltonian density of the gapless edge channels of the decoupled system is given by

$$\mathcal{H}_0 = \frac{2v_\rho}{4\pi}\sum_{j=1}^{\infty}[(\partial_x\phi_{\rho,j,L})^2 + (\partial_x\phi_{\rho,j,R})^2] + iv_\psi\sum_{j=1}^{\infty}(\psi_{j,L}\partial_x\psi_{j,L} - \psi_{j,R}\partial_x\psi_{j,R}). \tag{109}$$

Here, v_ρ and v_ψ denote the speeds of the charged mode ϕ_ρ and the Majorana mode ψ, respectively. The subscripts L and R label the left and right chiralities of the modes. The integer index j labels the quantum Hall stripes. The commutation relations of the Majorana fermions are $\{\psi_{j,D}(x), \psi_{i,D'}(x')\} = \frac{1}{2}\delta(x-x')\delta_{ij}\delta_{DD'}$, where D and D' can be R and L.

Let us summarize the idea of the construction. Recall that the PH-Pfaffian and Pfaffian states are related by neutral-mode flipping. As shown in Fig. 12, the couplings between the stripes gap out pairs of modes and leave a single gapless charged mode and a single gapless Majorana mode at the edge of the system. Furthermore, this Majorana mode has the opposite chirality to that of the gapless boson. Thus, the gapless edge acquires the structure demanded by the PH-Pfaffian order. Hence, an effective Hamiltonian for the PH-Pfaffian order is constructed.

Explicitly, we first gap out charged modes by introducing *electron-pair* tunneling between neighboring stripes (step 1 in Fig. 12). The coupling is described by the following Hamilto-

TABLE VI. Experimental signatures of different topological orders in the sixteenfold way. The second column provides the Chern number of the edge, which should equal the Chern number of the bulk. A non-Abelian (Abelian) order has an odd (even) Chern number. The states with negative ν_C have upstream neutral modes. For all topological orders, the most fundamental quasiparticle has the charge $q = e/4$. The fifth to seventh columns give the universal tunneling exponents for different types of quasiparticles, with the most relevant one being boldfaced. The eighth column provides the thermal Hall conductance coefficients, which are half-integers (integers) for non-Abelian orders (Abelian orders). In the last three columns, we list the expected results from interferometry. The bottom three entries in the last two columns refer to the situation in which the dominant process is $e/2$ tunneling. Everywhere else, we assume that the dominant quasiparticle has the charge $e/4$. All non-Abelian orders should demonstrate even-odd effect in a Fabry-Pérot interferometer. Abelian orders (except the $K = 8$ state) may also show the same effect, if they possess flavor symmetry. The last two columns list the maximal and minimal values of the Fano factor in a shot-noise experiment with a symmetric Mach-Zehnder interferometer ($s = 1$).

Name	ν_C	Non-Abelian?	q	$g_{e/4}$	$g_{e/2}$	g_e	κ_H	Even-odd effect?	$(e^*/e)_{\max}$	$(e^*/e)_{\min}$
$K = 8$	0	No	$e/4$	**1/8**	1/2	∞	3	No	2	11/16
Pfaffian	1	Yes	$e/4$	**1/4**	1/2	3	3.5	Yes	3.20	0.44
PH-Pfaffian	−1	Yes	$e/4$	**1/4**	1/2	3	2.5	Yes	∞	1/2
331	2	No	$e/4$	**3/8**	1/2	3	4	Maybe	1.39	0.39
113	−2	No	$e/4$	**3/8**	1/2	3	2	Maybe	13.5	0.38
$SU(2)_2$	3	Yes	$e/4$	**1/2**	**1/2**	3	4.5	Yes	1	3/8
Anti-Pfaffian	−3	Yes	$e/4$	**1/2**	**1/2**	3	1.5	Yes	3.20	0.44
$\nu_C = 4$	4	No	$e/4$	5/8	**1/2**	3	5	Maybe	1.39	0.39
Anti-331	−4	No	$e/4$	5/8	**1/2**	3	1	Maybe	1.39	0.39
$\nu_C = 5$	5	Yes	$e/4$	3/4	**1/2**	3	5.5	Yes	3.20	0.44
Anti-$SU(2)_2$	−5	Yes	$e/4$	3/4	**1/2**	3	0.5	Yes	1	3/8
$\nu_C = 6$	6	No	$e/4$	7/8	**1/2**	3	6	Maybe	13.5	0.38
$\nu_C = -6$	−6	No	$e/4$	7/8	**1/2**	3	0	Maybe	1.39	0.39
$\nu_C = 7$	7	Yes	$e/4$	1	**1/2**	3	6.5	Yes	1	1/2
$\nu_C = -7$	−7	Yes	$e/4$	1	**1/2**	3	−0.5	Yes	1	1/2
$\nu_C = 8$	8	No	$e/4$	9/8	**1/2**	3	7	Maybe	1	1/2

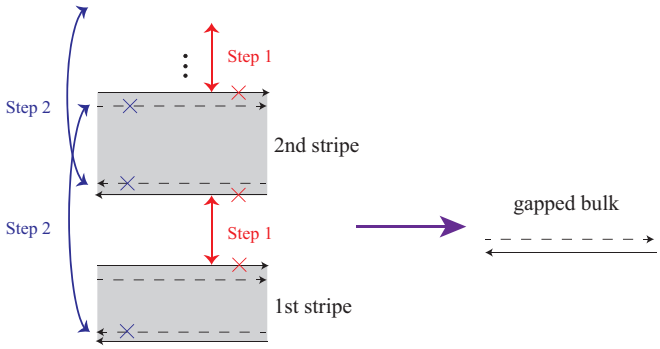

FIG. 12. Coupled-stripe construction of the effective Hamiltonian for the PH-Pfaffian order from a collection of quantum Hall stripes in the Pfaffian state. The solid lines (the dashed lines) refer to the charged bosonic modes (Majorana fermions). The lines with arrows on both ends represent inter-stripe interactions which gap out the pairs of the modes, connected by those lines.

nian density:

$$\mathcal{H}_1 = \Gamma_1 \sum_{j=1}^{\infty} (\psi_{j,R} e^{2i\phi_{\rho,j,R}})^2 (\psi_{j+1,L} e^{-2i\phi_{\rho,j+1,L}})^2 + \text{H.c.}$$
$$= 2\Gamma_1 \sum_{j=1}^{\infty} \cos(4\phi_{\rho,j,R} - 4\phi_{\rho,j+1,L}). \quad (110)$$

Here, we have used the property that ψ^2 is a c number. This number is dimensional, so, strictly speaking, the constants Γ_1 are not identical on the two sides of Eq. (110). This minor point is of no importance below. Note that we can add a density-density interaction $w\partial_x\phi_{\rho,j,R}\partial_x\phi_{\rho,j+1,L}$ that makes the tunneling (110) relevant in the renormalization group sense. As always with coupled-wire constructions, it is essential that the arguments commute for any two cosines (or any one cosine in different points) in Eq. (110):

$$[4[\phi_{\rho,j,R}(x) - \phi_{\rho,j+1,L}(x)], 4[\phi_{\rho,i,R}(y) - \phi_{\rho,i+1,L}(y)]] = 0 \quad (111)$$

for any i, j, x, and y. As a consequence, it may be legitimate to treat the arguments of the cosines as c numbers.

When a negative Γ_1 is sufficiently large, the combination $4\phi_{\rho,j,R} - 4\phi_{\rho,j+1,L}$ is pinned to a multiple of 2π. This gaps out the modes $\phi_{\rho,j,R}$ and $\phi_{\rho,j+1,L}$. Only $\phi_{\rho,1,L}$ is not coupled with a right-moving mode by the above tunneling operator and hence $\phi_{\rho,1,L}$ remains gapless. Next, the Majorana modes are gapped out by the following coupling (step 2 in Fig. 12):

$$\mathcal{H}_2 = \Gamma_2 \sum_{j=1}^{\infty} (\psi_{j,L} e^{2i\phi_{\rho,j,R}})(\psi_{j+1,R} e^{-2i\phi_{\rho,j+1,L}}) + \text{H.c.}$$
$$= \Gamma_2 \sum_{j=1}^{\infty} \psi_{j,L}\psi_{j+1,R} e^{2i(\phi_{\rho,j,R} - \phi_{\rho,j+1,L})} + \text{H.c.} \quad (112)$$

We must explain why such coupling is legitimate. Two requirements must be satisfied. First, the interaction must conserve the electric charge as it obviously does. Second, it should conserve the topological charge. To understand why the second condition is satisfied, observe that the above tunneling interaction consists of products of operators of the type $\psi_{j,L}\exp(2i\phi_{\rho,j,R}) = \hat{A}\hat{B}$ with $\hat{A} = \psi_{j,L}\exp(2i\phi_{\rho,j,L})$ and $\hat{B} = \exp(2i\phi_{\rho,j,R} - 2i\phi_{\rho,j,L})$. $\hat{A}$ is a topologically trivial electron operator. $\hat{B}$ transfers one electron charge between the two sides of a single stripe and hence is also topologically trivial. Hence, the product of $\hat{A}$ and $\hat{B}$ also conserves the topological charge, as does the interaction (112).

At this point, we observe that the combination of the charged modes $4\phi_{\rho,j,R} - 4\phi_{\rho,j+1,L}$ was fixed to be a multiple of 2π at the first step. Hence, the exponential factor $\exp[2i(\phi_{\rho,j,R} - \phi_{\rho,j+1,L})]$ in Eq. (112) is ± 1. As a consequence, $\mathcal{H}_2$ can be simplified into

$$\mathcal{H}_2 = \tilde{\Gamma}_2 \sum_{j=1}^{\infty} \psi_{j,L}\psi_{j+1,R} + \text{H.c.}, \quad (113)$$

where the $\pm$ sign factor is absorbed into $\tilde{\Gamma}_2$. To make sure that $\tilde{\Gamma}_2$ is the same for all j, one may also need to redefine $\psi_{j,L} \to -\psi_{j,L}$.

The overall Hamiltonian density of the coupled system $\mathcal{H} = \mathcal{H}_0 + \mathcal{H}_1 + \mathcal{H}_2$ can be separated into the bulk and edge parts: $\mathcal{H} = \mathcal{H}_b + \mathcal{H}_e$. The gapped bulk contribution is

$$\mathcal{H}_b = \frac{4v_\rho}{4\pi} \sum_{j=1}^{\infty} [(\partial_x\theta_j)^2 + (\partial_x\varphi_j)^2] + 2\Gamma_1 \sum_{j=1}^{\infty} \cos(8\varphi_j)$$
$$+ iv_\psi \sum_{j=1}^{\infty} (\psi_{j,L}\partial_x\psi_{j,L} - \psi_{j+1,R}\partial_x\psi_{j+1,R})$$
$$+ \tilde{\Gamma}_2 \sum_{j=1}^{\infty} \psi_{j,L}\psi_{j+1,R} + \text{H.c.}, \quad (114)$$

where

$$\theta_j = (\phi_{\rho,j,R} + \phi_{\rho,j+1,L})/2, \quad (115)$$

$$\varphi_j = (\phi_{\rho,j,R} - \phi_{\rho,j+1,L})/2. \quad (116)$$

The edge contribution $\mathcal{H}_e$ is gapless.

To verify that the bulk is gapped, we need to check that the Majorana modes in Eq. (114) are gapped out. We expand the Majorana operators as superpositions of plane waves:

$$\psi_{j,L}(x) = \frac{1}{\sqrt{L}} \sum_k a_{j,k} e^{ikx}, \quad (117)$$

$$\psi_{j,R}(x) = \frac{1}{\sqrt{L}} \sum_k \tilde{a}_{j,k} e^{ikx}, \quad (118)$$

where L is the length of the stripes. The condition $\psi(x) = \psi^\dagger(x)$ implies that $a_{j,-k} = a^\dagger_{j,k}$. The anticommutation relations for $a_{j,k}$ and $\tilde{a}_{j,k}$ are

$$\{a_{i,k}, a^\dagger_{j,k'}\} = \tfrac{1}{2}\delta_{i,j}\delta_{k,k'}, \quad (119)$$

$$\{\tilde{a}_{i,k}, \tilde{a}^\dagger_{j,k'}\} = \tfrac{1}{2}\delta_{i,j}\delta_{k,k'}, \quad (120)$$

$$\{a_{i,k}, \tilde{a}^\dagger_{j,k'}\} = 0. \quad (121)$$

The Hamiltonian of the bulk Majorana degrees of freedom is given by the integral $H_\psi = \int_0^L dx\, \mathcal{H}_{b\psi}$, where $\mathcal{H}_{b\psi}$ is the sum of the last two rows in Eq. (114). With the new notation $a_{j,k}$, $\tilde{a}_{j,k}$, the Hamiltonian H_ψ can be rewritten as

$$H_\psi = 2v_\psi \sum_{j=1}^{\infty}\sum_{k>0} k(\tilde{a}^\dagger_{j+1,k}\tilde{a}_{j+1,k} - a^\dagger_{j,k}a_{j,k}) + \left[\tilde{\Gamma}_2 \sum_{j=1}^{\infty}\sum_{k>0}(a^\dagger_{j,k}\tilde{a}_{j+1,k} - \tilde{a}^\dagger_{j+1,k}a_{j,k}) + \text{H.c.}\right]. \tag{122}$$

Then, H_ψ can be diagonalized by the following transformation:

$$c_{j,k} = \frac{(\lambda - v_\psi k)a_{j,k} + i\,\mathrm{Im}(\tilde{\Gamma}_2)\tilde{a}_{j+1,k}}{\sqrt{[\mathrm{Im}(\tilde{\Gamma}_2)]^2 + (v_\psi k - \lambda)^2}}, \tag{123}$$

$$d_{j,k} = \frac{i\,\mathrm{Im}(\tilde{\Gamma}_2)a_{j,k} + (\lambda - v_\psi k)\tilde{a}_{j+1,k}}{\sqrt{[\mathrm{Im}(\tilde{\Gamma}_2)]^2 + (v_\psi k - \lambda)^2}}, \tag{124}$$

where $\lambda = \sqrt{(v_\psi k)^2 + [\mathrm{Im}(\tilde{\Gamma}_2)]^2}$. The anticommutation relations for $c_{j,k}$ and $d_{j,k}$ are the same as the relations for $a_{j,k}$ and $\tilde{a}_{j,k}$. The above transformation leads to the following diagonalized H_ψ:

$$H_\psi = 2\sum_{j=1}^{\infty}\sum_{k>0}\sqrt{v_\psi^2 k^2 + [\mathrm{Im}(\tilde{\Gamma}_2)]^2}\,(c^\dagger_{j,k}c_{j,k} - d^\dagger_{j,k}d_{j,k}). \tag{125}$$

It is now evident that as long as $\mathrm{Im}(\tilde{\Gamma}_2) \neq 0$, the Majorana modes are gapped with the gap of $|\mathrm{Im}(\tilde{\Gamma}_2)|$.

The bulk Hamiltonian is thus gapped:

$$\begin{aligned}\int dx\,\mathcal{H}_b = {}& \frac{4v_\rho}{4\pi}\int dx \sum_{j=1}^{\infty}[(\partial_x\theta_j)^2 + (\partial_x\varphi_j)^2] \\ & + 2\Gamma_1 \int dx \sum_{j=1}^{\infty}\cos(8\varphi_j) \\ & + 2\sum_{j=1}^{\infty}\sum_{k>0}\sqrt{v_\psi^2 k^2 + [\mathrm{Im}(\tilde{\Gamma}_2)]^2} \\ & \times (c^\dagger_{j,k}c_{j,k} - d^\dagger_{j,k}d_{j,k}).\end{aligned} \tag{126}$$

At the same time, the modes $\phi_{\rho,1,L}$ and $\psi_{1,R}$ remain gapless and are described by the edge Hamiltonian $\int dx\,\mathcal{H}_e$:

$$\mathcal{H}_e = \frac{2v_\rho}{4\pi}(\partial_x\phi_{\rho,1,L})^2 - iv_\psi\psi_{1,R}\partial_x\psi_{1,R}. \tag{127}$$

This is the edge theory of the PH-Pfaffian order. The electron operator

$$\begin{aligned}\Psi_e &\sim \exp(2i\phi_{\rho,1,L})\psi_{1,L}[\psi_{1,L}\psi_{1,R}] \\ &\sim \exp(2i\phi_{\rho,1,L})\psi_{1,R}.\end{aligned} \tag{128}$$

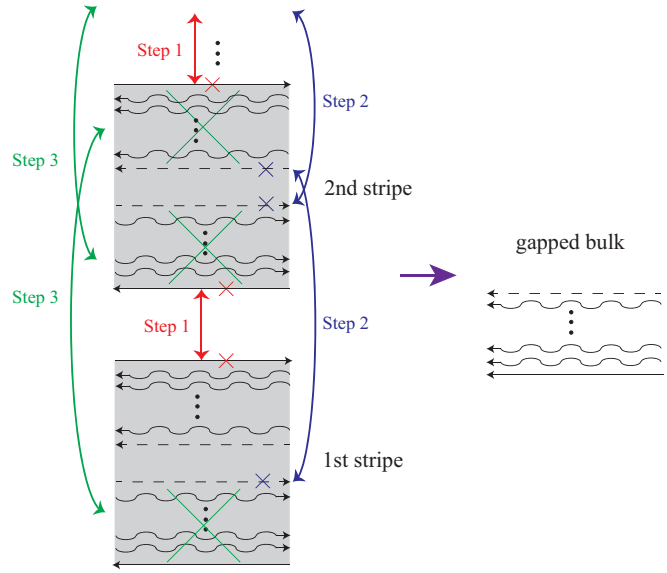

FIG. 13. Coupled-stripe construction for neutral-mode flipping in non-Abelian topological orders. The charged modes, the Majorana modes, and the bosonic neutral modes are denoted by solid lines, dashed lines, and wavy lines, respectively. Three different tunneling processes between neighboring stripes are introduced to gap out the modes in the bulk of the system. The remaining gapless edge modes are shown in the right panel.

B. First coupled-stripe construction (CW1) for non-Abelian topological orders

The previous construction can be generalized to relate other non-Abelian topological orders which possess neutral bosonic modes or, equivalently, more than one Majorana mode at the edge. Below, we will use the language of a single Majorana edge mode. The K matrices, describing the Abelian edge modes, take the form (7) with the corresponding charge vector $t = (1, 0, \ldots, 0)^T$.

We are going to introduce coupled-stripe constructions of two types. The first construction describes neutral-mode flipping. The second construction describes particle-hole conjugation. We will call these two constructions CW1. A different approach CW2 to the coupled-stripe construction will be considered in the next subsection.

1. Effective coupled-stripe construction for neutral-mode flipping

Our goal is to transform a system with the Chern number $-\nu_C < 0$ into a system with the opposite Chern number ν_C. As shown in Fig. 13, we start with a system of decoupled quantum Hall stripes. Each edge of each stripe contains a single downstream charged mode, one upstream Majorana mode, and N upstream bosonic neutral modes so that $-\nu_C = -(2N+1)$. The velocities of all upstream modes are the same. By introducing electron tunneling processes between neighboring stripes, we gap out pairs of the modes. At the end, gapless modes remain only at the topmost and bottommost edges of the system of the stripes. The structure of the gapless modes corresponds to the desired Chern number ν_C.

The Hamiltonian density of decoupled stripes with no interstripe tunneling is given by

$$\begin{aligned}\mathcal{H}_0 = &\frac{2v_\rho}{4\pi}\sum_{j=1}^{\infty}[(\partial_x\phi_{\rho,j,L})^2+(\partial_x\phi_{\rho,j,R})^2]\\ &+\frac{v_n}{4\pi}\sum_{j=1}^{\infty}\sum_{i=1}^{N}[(\partial_x\phi_{n_i,j,L})^2+(\partial_x\phi_{n_i,j,R})^2]\\ &+iv_n\sum_{j=1}^{\infty}(\psi_{j,L}\partial_x\psi_{j,L}-\psi_{j,R}\partial_x\psi_{j,R}),\end{aligned}\tag{129}$$

where v_ρ labels the speed of the charged mode, v_n is the speed of the neutral modes. The subsubscript i in ϕ_{n_i} ranges from 1 to N and enumerates the N neutral bosonic modes at the edge of each stripe.

As in Sec. VII A, the charged modes are gapped out by introducing electron-pair tunneling between neighboring stripes (step 1 in Fig. 13):

$$\begin{aligned}\mathcal{H}_1 &= \Gamma_1\sum_{j=1}^{\infty}(\psi_{j,L}e^{2i\phi_{\rho,j,R}})^2(\psi_{j+1,R}e^{-2i\phi_{\rho,j+1,L}})^2+\text{H.c.}\\ &= 2\Gamma_1\sum_{j=1}^{\infty}\cos(4\phi_{\rho,j,R}-4\phi_{\rho,j+1,L}).\end{aligned}\tag{130}$$

Notice that the Majorana mode and the charged mode in the electron operator have opposite chiralities as the topological order has a negative Chern number (for example, PH-Pfaffian or anti-Pfaffian). The coupling constant Γ_1 is set to a sufficiently large negative number to make sure that the charged modes are gapped in the bulk of the system.

Next, we proceed to gap out the Majorana modes in the bulk by adding single-electron tunneling (step 2 in Fig. 13):

$$\begin{aligned}\mathcal{H}_2 &= \Gamma_2\sum_{j=1}^{\infty}(\psi_{j,R}e^{2i\phi_{\rho,j,R}})(\psi_{j+1,L}e^{-2i\phi_{\rho,j+1,L}})+\text{H.c.}\\ &= \tilde{\Gamma}_2\sum_{j=1}^{\infty}\psi_{j,R}\psi_{j+1,L}+\text{H.c.}\end{aligned}\tag{131}$$

The neutral bosonic modes in the bulk can be gapped by an additional interstripe tunneling as shown as step 3 in Fig. 13. Recall that $\Psi_e = e^{-i\phi_{n_i}}e^{2i\phi_\rho}$ is a legitimate electron operator for any $i = 1, 2, \ldots, N$. Thus, by analogy with Eq. (131), one can consider the following electron tunneling process:

$$\begin{aligned}\mathcal{H}_3 = &\Gamma_3\sum_{j=1}^{\infty}\sum_{i=1}^{N}(e^{-i\phi_{n_i,j,R}}e^{2i\phi_{\rho,j,R}})\\ &\times(e^{i\phi_{n_i,j+1,L}}e^{-2i\phi_{\rho,j+1,L}})+\text{H.c.}\\ = &\,2\tilde{\Gamma}_3\sum_{j=1}^{\infty}\sum_{i=1}^{N}\cos(\phi_{n_i,j+1,L}-\phi_{n_i,j,R}).\end{aligned}\tag{132}$$

All modes in the coupled stripes are completely gapped out by the above three tunneling processes, except for the modes which do not appear in $\mathcal{H}_1$, $\mathcal{H}_2$, and $\mathcal{H}_3$. As a result, the effective Hamiltonian for the gapped bulk is given by

$$\begin{aligned}H_b = &\int\mathcal{H}_b\,dx\\ = &\frac{4v_\rho}{4\pi}\int\sum_{j=1}^{\infty}[(\partial_x\theta_{\rho,j})^2+(\partial_x\varphi_{\rho,j})^2]\,dx\\ &+2\Gamma_1\int\sum_{j=1}^{\infty}\cos(8\varphi_{\rho,j})\,dx\\ &+\frac{2v_n}{4\pi}\int\sum_{j=1}^{\infty}\sum_{i=1}^{N}[(\partial_x\theta_{n_i,j})^2+(\partial_x\varphi_{n_i,j})^2]\,dx\\ &+2\tilde{\Gamma}_3\int\sum_{j=1}^{\infty}\sum_{i=1}^{N}\cos(2\varphi_{n_i,j})\,dx\\ &+2\sum_{j=1}^{\infty}\sum_{k>0}\sqrt{k^2v_n^2+\text{Im}(\tilde{\Gamma}_2)^2}(c_{j,k}^\dagger c_{j,k}-d_{j,k}^\dagger d_{j,k}),\end{aligned}\tag{133}$$

where

$$\varphi_{n_i,j} = (\phi_{n_i,j+1,L}-\phi_{n_i,j,R})/2;\tag{134}$$

$$\theta_{n_i,j} = (\phi_{n_i,j+1,L}+\phi_{n_i,j,R})/2;\tag{135}$$

$$\varphi_{\rho,j} = (\phi_{\rho,j+1,L}-\phi_{\rho,j,R})/2;\tag{136}$$

$$\theta_{\rho,j} = (\phi_{\rho,j+1,L}+\phi_{\rho,j,R})/2.\tag{137}$$

The Hamiltonian density of the gapless edge at the bottom of the system of the stripes is

$$\mathcal{H}_e = \frac{2v_\rho}{4\pi}(\partial_x\phi_{\rho,1,L})^2+\frac{v_n}{4\pi}\sum_{i=1}^{N}\left(\partial_x\phi_{n_i,1,L}\right)^2+iv_n\psi_{1,L}\partial_x\psi_{1,L}.\tag{138}$$

The chirality of the gapless neutral modes at the edge is opposite to that of the neutral modes in the original state. Hence, the topological orders with the Chern numbers ν_C and $-\nu_C$ can be related by the above coupled-stripe construction. This relationship is illustrated by horizontal arrows in Fig. 1. The electron operators on the edge

$$\begin{aligned}\Psi_\psi &\sim \exp(2i\phi_{\rho,1,L})\psi_{1,R}[\psi_{1,R}\psi_{1,L}]\\ &\sim \exp(2i\phi_{\rho,1,L})\psi_{1,L};\end{aligned}\tag{139}$$

$$\begin{aligned}\Psi_n &\sim \exp(2i\phi_{\rho,1,L})\exp(i\phi_{n_i,1,R})\\ &\quad\times\left[\exp\left(-i\phi_{n_i,1,R}\right)\exp\left(i\phi_{n_i,1,L}\right)\right]\\ &\sim \exp(2i\phi_{\rho,1,L})\exp(i\phi_{n_i,1,L}).\end{aligned}\tag{140}$$

2. *Effective coupled-stripe construction for particle-hole conjugation*

Another connection among the orders in the sixteenfold way is particle-hole conjugation. For example, the Pfaffian and anti-Pfaffian orders are particle-hole conjugates. As shown in Fig. 14, we consider a collection of alternating stripes in the $\nu = 1$ IQH state and in the $\nu = \frac{1}{2}$ FQH state

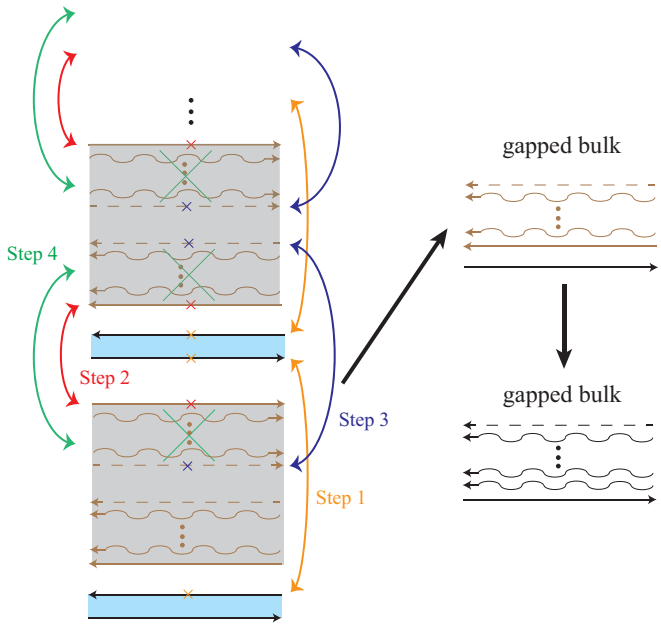

FIG. 14. Effective coupled-stripe construction for particle-hole conjugation of a topological order with filling factor $\nu = \frac{1}{2}$. In the left panel, the system consists of $\nu = 1$ integer quantum Hall stripes (narrow) and $\nu = \frac{1}{2}$ fractional quantum Hall stripes (wide), arranged in an alternating pattern. The upper right panel shows the resulting gapless edge structure after turning on tunneling between the stripes. The lower right panel is the edge structure in the presence of a density-density interaction on the edge.

to formulate a coupled-stripe construction for particle-hole conjugation.

We begin by gapping out the modes from the $\nu = 1$ IQH stripes with the following electron tunneling process:

$$\begin{aligned}\mathcal{H}_1 &= \frac{\Gamma_1}{2} e^{i\phi^{\nu=1}_{\rho,j,L}} e^{-i\phi^{\nu=1}_{\rho,j+1,R}} + \text{H.c.} \\ &= \Gamma_1 \cos\left(\phi^{\nu=1}_{\rho,j,L} - \phi^{\nu=1}_{\rho,j+1,R}\right). \end{aligned} \tag{141}$$

Here, $\phi^{\nu=1}_{\rho,j,L/R}$ denotes the charged mode in the jth $\nu = 1$ stripe. As illustrated in Fig. 14, the coupling gaps out the modes in the bulk of our system but leaves a single gapless charged mode $\phi^{\nu=1}_{\rho,1,R}$ at the edge of the first stripe.

The modes in the $\nu = \frac{1}{2}$ FQH stripes can be gapped out by coupling the stripes in the same way as in the previous construction for neutral-mode flipping. We introduce three tunneling terms $\mathcal{H}_2$, $\mathcal{H}_3$, and $\mathcal{H}_4$:

$$\begin{aligned}\mathcal{H}_2 &= \Gamma_2 \sum_{j=1}^{\infty} \left(\psi_{j,R} e^{2i\phi^{\nu=1/2}_{\rho,j,R}}\right)^2 \left(\psi_{j+1,L} e^{-2i\phi^{\nu=1/2}_{\rho,j+1,L}}\right)^2 + \text{H.c.} \\ &= 2\Gamma_2 \sum_{j=1}^{\infty} \cos\left(4\phi^{\nu=1/2}_{\rho,j,R} - 4\phi^{\nu=1/2}_{\rho,j+1,L}\right) \end{aligned} \tag{142}$$

gaps out the charged modes,

$$\begin{aligned}\mathcal{H}_3 &= \Gamma_3 \sum_{j=1}^{\infty} \left(\psi_{j,R} e^{2i\phi^{\nu=1/2}_{\rho,j,R}}\right)\left(\psi_{j+1,L} e^{-2i\phi^{\nu=1/2}_{\rho,j+1,L}}\right) + \text{H.c.} \\ &= \tilde{\Gamma}_3 \sum_{j=1}^{\infty} \psi_{j,R}\psi_{j+1,L} + \text{H.c.} \end{aligned} \tag{143}$$

gaps out the Majorana modes,

$$\begin{aligned}\mathcal{H}_4 &= \Gamma_4 \sum_{j=1}^{\infty}\sum_{i=1}^{N} \left(e^{-i\phi^{\nu=1/2}_{n_i,j,R}} e^{2i\phi^{\nu=1/2}_{\rho,j,R}}\right)\left(e^{i\phi^{\nu=1/2}_{n_i,j+1,L}} e^{-2i\phi^{\nu=1/2}_{\rho,j+1,L}}\right) + \text{H.c.} \\ &= 2\tilde{\Gamma}_4 \sum_{j=1}^{\infty}\sum_{i=1}^{N} \cos\left(\phi^{\nu=1/2}_{n_i,j+1,L} - \phi^{\nu=1/2}_{n_i,j,R}\right) \end{aligned} \tag{144}$$

gaps out the bosonic neutral modes. After the introduction of the couplings $\mathcal{H}_{1,2,3,4}$, only the integer charged mode $\phi^{\nu=1}_{\rho,1,R}$, and the fractional modes $\phi^{\nu=1/2}_{\rho,1,L}$, $\phi^{\nu=1/2}_{n_i,1,L}$, and $\psi_{1,L}$ remain gapless at the edge. This edge structure is shown in the upper right panel in Fig. 14.

To complete our procedure, we add a density-density interaction of the two charged modes $\phi^{\nu=1}_{\rho,1,R}$ and $\phi^{\nu=1/2}_{\rho,1,L}$. Its energy density is

$$\mathcal{H}_w = \frac{2w}{4\pi} \partial_x \phi^{\nu=1}_{\rho,1,R} \partial_x \phi^{\nu=1/2}_{\rho,1,L}. \tag{145}$$

The two charged modes decouple from the rest of the modes. The Lagrangian density of the charged modes becomes

$$\begin{aligned}\mathcal{L} = &-\frac{1}{4\pi}\left[\partial_t \phi^{\nu=1}_{\rho,1,R} \partial_x \phi^{\nu=1}_{\rho,1,R} + v_1 \left(\partial_x \phi^{\nu=1}_{\rho,1,R}\right)^2\right] \\ &+ \frac{2}{4\pi}\left[\partial_t \phi^{\nu=1/2}_{\rho,1,L} \partial_x \phi^{\nu=1/2}_{\rho,1,L} - v_{1/2} \left(\phi^{\nu=1/2}_{\rho,1,L}\right)^2\right] \\ &- \frac{2w}{4\pi} \partial_x \phi^{\nu=1}_{\rho,1,R} \partial_x \phi^{\nu=1/2}_{\rho,1,L}. \end{aligned} \tag{146}$$

We introduce a new charged mode $\phi_\rho = \phi^{\nu=1}_{\rho,1,R} - \phi^{\nu=1/2}_{\rho,1,L}$ and a new neutral mode $\phi_{N+1} = \phi^{\nu=1}_{\rho,1,R} - 2\phi^{\nu=1/2}_{\rho,1,L}$. We also choose $w = -2(v_1 + v_{1/2})/3$ and $v_1 = 2v_{1/2} - 3v_n$. The action then becomes

$$\begin{aligned}\mathcal{L} = &-\frac{2}{4\pi}[\partial_t \phi_\rho \partial_x \phi_\rho + v_\rho (\partial_x \phi_\rho)^2] \\ &+ \frac{1}{4\pi}[\partial_t \phi_{N+1} \partial_x \phi_{N+1} - v_n (\partial_x \phi_{N+1})^2], \end{aligned} \tag{147}$$

where v_n is the same velocity as the speed of the rest of the neutral modes, and $v_\rho = v_{1/2} - 2v_n$. To make sure that the Hamiltonian is positive definite, we assume that $v_\rho, v_{1/2}, v_1 \gg v_n$. The action (147) shows two decoupled modes. Adding the rest of the neutral modes, we arrive to the edge structure, depicted in the lower right panel of Fig. 14. This corresponds to the contribution of any of the edges of the stripes to Eq. (129). This was precisely our goal. The structure of the allowed electron operators on the edge remains the same as before the tunneling between the stripes was turned on since the gapless edge structure is simply inherited from the lowest edges of the lowest wide and narrow stripes in Fig. 14.

C. Second coupled-stripe construction CW2 for non-Abelian topological orders

Here, we provide a short discussion of another iterative coupled-stripe construction to relate different non-Abelian orders of the sixteenfold way. This construction is called CW2 in Fig. 1. It differs from CW1 in two ways. First, neutral bosonic modes are gapped out in a different way on step 3

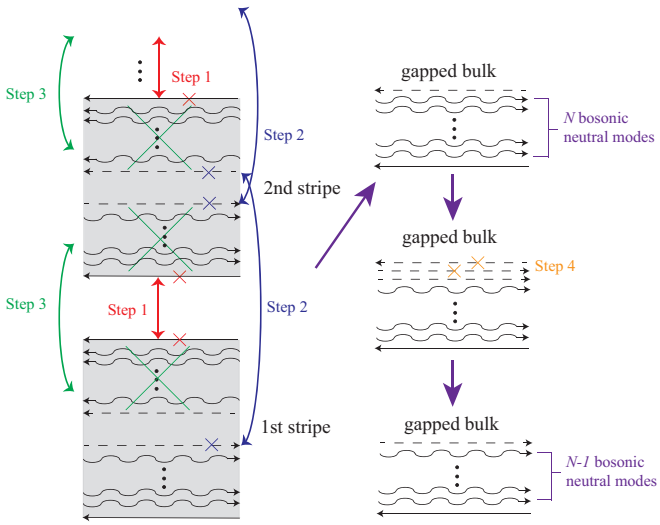

FIG. 15. Second coupled-stripe construction (CW2) for non-Abelian topological orders of the sixteenfold way. On step 4, we fermionize a neutral bosonic mode into two Majorana fermions, then gap out one of them by coupling it to the counterpropagating Majorana mode. Thus, the number of the bosonic neutral modes decreases by one.

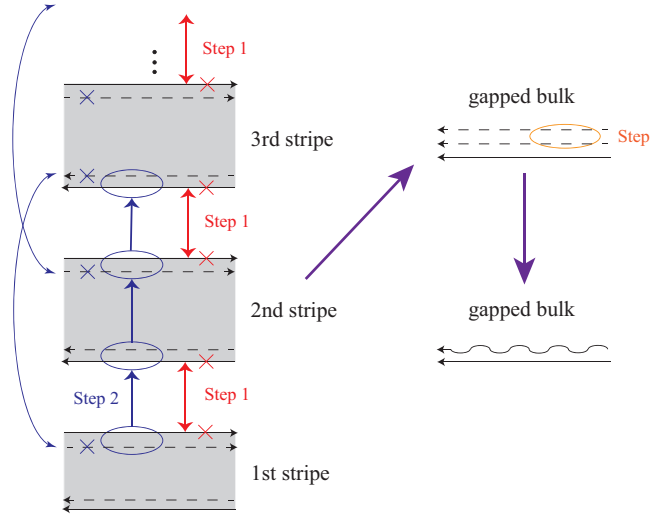

FIG. 16. Coupled-stripe construction for the Abelian 331 order from a collection of quantum Hall stripes in the Pfaffian state. On step 3, two copropagating Majorana modes form one neutral bosonic mode.

(cf. step 3 in Figs. 13 and 15). Second, an additional step 4 is introduced.

After the coupling of the Hall stripes with three tunneling processes as shown in Fig. 15, a gapless Majorana mode is left at the edge. Its propagation direction is opposite to the direction of the remaining gapless neutral Bose modes. This "wrongly moving" mode can be gapped out by coupling it to a Majorana mode obtained by fermionizing one of the neutral bosonic modes at the edge. Indeed, a Bose mode can be seen as two copropagating Majoranas. As a result, this construction reduces the number of the bosonic neutral modes by one. Thus, it provides a way to relate the effective Hamiltonians of the orders from the sixteenfold way with the Chern numbers ν_C and $\nu_C - 2$, as shown in Fig. 1.

D. Coupled-stripe construction for Abelian topological orders

A coupled-stripe construction can also be employed to construct effective Hamiltonians for the Abelian orders from the sixteenfold way. We first construct an effective Hamiltonian for the 331 order from the Pfaffian order. After this is done, the same tricks as in the previous subsection produce effective Hamiltonians for all the other Abelian orders.

1. Pfaffian order and 331 order

In Fig. 16, we illustrate the coupled-stripe system and the corresponding couplings for constructing the 331 order from the Pfaffian state. On step 1, charged modes are gapped out by the tunneling operator from Eq. (110). Since the edge of the 331 liquid has one downstream neutral bosonic mode which is equivalent to two downstream Majorana modes, the Majorana modes in the stripes should be gapped by coupling the jth stripe and the $(j+2)$th stripe on step 2 as shown in the figure. More precisely, we introduce transfer of a pair of electrons among three stripes j, $j+1$, $j+2$. The Hamiltonian density of the tunneling term is

$$\begin{aligned}\mathcal{H}_2 &= \Gamma_2 \sum_{j=1}^{\infty} [(\psi_{j,R} e^{2i\phi_{\rho,j,R}})(\psi_{j+1,L} e^{-2i\phi_{\rho,j+1,L}})][\psi_{j+1,L}\psi_{j+1,R}] \\ &\quad \times [(\psi_{j+1,R} e^{2i\phi_{\rho,j+1,R}})(\psi_{j+2,L} e^{-2i\phi_{\rho,j+2,L}})] + \text{H.c.} \\ &= \tilde{\Gamma}_2 \sum_{j=1}^{\infty} \psi_{j,R}\psi_{j+2,L} + \text{H.c.} \end{aligned} \tag{148}$$

This operator is allowed since it conserves the total electric charge and the topological charge. Indeed, all four expressions in the parentheses are topologically trivial electron operators. The middle square brackets transfer a Majorana fermion between the edges of the same stripe and hence is allowed.

Steps 1 and 2 gap out all modes, except for $\phi_{\rho,1,L}$, $\psi_{1,L}$, and $\psi_{2,L}$. Notice that the two gapless Majorana modes have the the same chirality. Hence, they can be combined to form a single Dirac fermion. In the bosonization language, it is equivalent to a bosonic neutral mode $\phi_{n,1,L}$. Finally, the effective Hamiltonian density for the edge modes is given by

$$\mathcal{H}_{\text{edge}} = \frac{2v_\rho}{4\pi}(\partial_x \phi_{\rho,1,L})^2 + \frac{v_n}{4\pi}(\partial_x \phi_{n,1,L})^2. \tag{149}$$

This is the edge structure of the 331 order. The electron operators can be chosen in the form

$$\begin{aligned}\Psi_e \sim\ & \exp(2i\phi_{\rho,1,L})\psi_{1,L}\{1 \pm i[\psi_{1,L}\psi_{1,R}] \\ & \times [\psi_{1,R}\cos(2[\phi_{\rho,1,R} - \phi_{\rho,2,L}])\psi_{2,L}]\} \end{aligned} \tag{150}$$

or, equivalently,

$$\Psi_e \sim \exp(2i\phi_{\rho,1,L})[\psi_{1,L} \pm i\psi_{2,L}]. \tag{151}$$

It is also possible to construct the Pfaffian state from the 331 state. We illustrate this by an example of a single stripe, as shown in Fig. 17. Our example only shows how to get the Pfaffian edge structure from the 331 edge structure. Multiple stripes are needed to produce the bulk Pfaffian order.

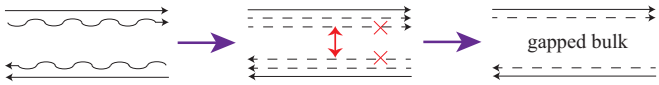

FIG. 17. Obtaining the edge structure of the Pfaffian state from the 331 state. For simplicity, we consider a single stripe. The bosonic neutral mode (wavy line) at the edge is fermionized into two Majorana modes (dashed lines). One of the Majorana modes couples with a Majorana mode on the opposite edge. The coupled Majorana modes are gapped out.

Recall that a bosonic neutral mode at the edge of the 331 state can be fermionized into two copropagating Majorana modes. Since quasiparticles can tunnel between the two opposite edges of the same quantum Hall liquid (but not across two different quantum Hall liquids), two counterpropagating Majorana modes can be directly coupled and gapped out. The resulting edge structure consists of a charged mode and one downstream Majorana mode on each edge. This is the edge structure of the Pfaffian state.

2. Iterative construction for other Abelian orders

In this section, we consider in detail the construction of the 113 order from the 331 order. The construction is very similar to the one we used in the non-Abelian case. We then briefly address a generalization to an arbitrary Abelian topological order.

The construction of the 113 order from the 331 order is parallel to the construction of PH-Pfaffian order from the Pfaffian order. We illustrate the construction in Fig. 18.

Since a Majorana mode is absent on the edges of Abelian stripes, the electron operators are $\hat{\Psi}_{\pm} = e^{\pm i\phi_n} e^{2i\phi_\rho}$. Here, ϕ_n can be any one of the neutral modes on the edge. Thus, it is possible to gap out the charged modes in the 331 quantum Hall stripes with the following interaction when Γ_1 is sufficiently strong:

$$\begin{aligned}\mathcal{H}_1 &= \Gamma_1 \sum_{j=1}^{\infty} [(e^{-i\phi_{n,j,R}} e^{2i\phi_{\rho,j,R}})(e^{i\phi_{n,j,R}} e^{2i\phi_{\rho,j,R}})] \\ &\quad \times [(e^{i\phi_{n,j+1,L}} e^{-2i\phi_{\rho,j,R}})(e^{-i\phi_{n,j,L}} e^{-2i\phi_{\rho,j,R}})] + \text{H.c.} \\ &= 2\Gamma_1 \sum_{j=1}^{\infty} \cos(4\phi_{\rho,j,R} - 4\phi_{\rho,j+1,L}). \end{aligned} \tag{152}$$

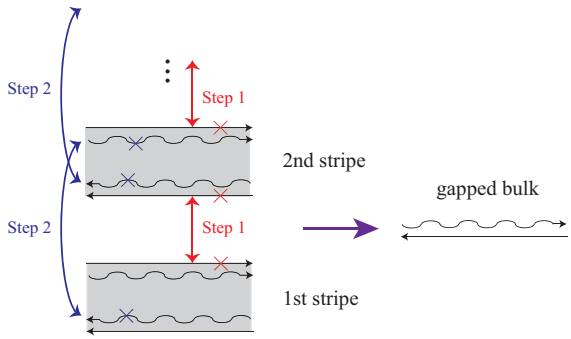

FIG. 18. Coupled-stripe construction for the 113 order from a collection of quantum Hall stripes in the 331 state. Here, the solid lines (wavy lines) represent the charged modes (neutral modes).

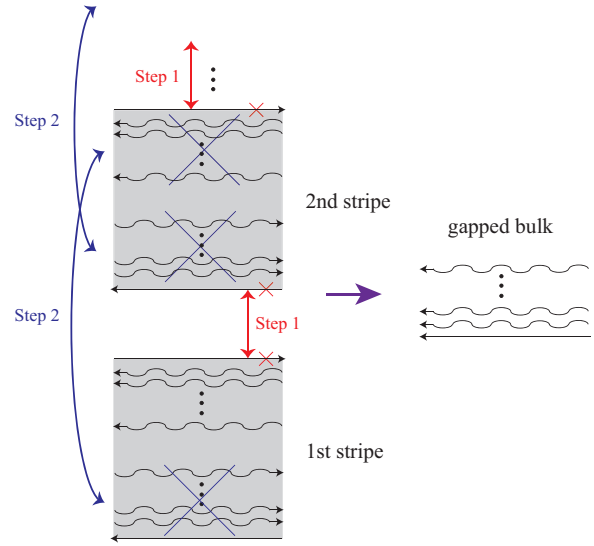

FIG. 19. Neutral-mode flipping construction for Abelian topological orders.

Next, we proceed to gap out the neutral modes in the bulk as shown in the figure (step 2). The corresponding interaction term is given by

$$\begin{aligned}\mathcal{H}_2 &= \Gamma_2 \sum_{j=1}^{\infty} (e^{-i\phi_{n,j,L}} e^{2i\phi_{\rho,j,R}})(e^{i\phi_{n,j+1,R}} e^{-2i\phi_{\rho,j+1,L}}) + \text{H.c.} \\ &= 2\tilde{\Gamma}_2 \sum_{j=1}^{\infty} \cos\phi_{n,j+1,R} - \phi_{n,j,L}). \end{aligned} \tag{153}$$

By gapping out the modes in the stripes with $\mathcal{H}_1$ and $\mathcal{H}_2$, one recovers the edge structure of the 113 order. Following the non-Abelian case, one can also easily verify that the correct structure of the electron operators on the edge is reproduced by this procedure.

For Abelian orders with more neutral modes on the edge, the same procedure can be applied to construct effective Hamiltonians for the topological order with the Chern number ν_C from a collection of stripes in the state with the Chern number $-\nu_C$ as shown in Fig. 19. The charged modes can be gapped out by the interaction from Eq. (152). Equation (132) shows a way to gap out the bulk neutral modes.

Aside from neutral-mode flipping (Fig. 19), we also need to perform particle-hole conjugation. The procedure is essentially identical to the non-Abelian case. The only important difference is that the interaction (152) is used to gap out fractional charged modes.

VIII. CONCLUSIONS

Composite fermions give an intuitive and powerful approach to FQHE. At odd-denominator filling factors, a difficult FQHE problem reduces to the much simpler integer QHE of composite fermions. In the latter problem, the single-particle spectrum is gapped. As a result, the basic properties of the QHE liquid are robust. In particular, similar physics is expected for a great variety of microscpic Hamiltonians. As long as the filling factor is the same, one can realistically

expect the same topological order in a complicated experimental system and in a system with a highly simplified Hamiltonian, suitable for numerical simulations.

Such picture cannot be generalized to half-integer filling factors, where the simplest application of the composite-fermion idea predicts a gapless liquid. This simplest behavior is compatible with the experiment at some filling factors but not at the others. This is not surprising since gapless states are not as robust as gapped ones. Indeed, a gapless liquid can be unstable to various weak interactions. Kitaev's classification reveals 16 instabilities which lead to 16 possible topological orders. All 16 orders are close relatives since they all emerge from Cooper pairing of the same type of composite fermions. Importantly, the existing numerical evidence does support a state of the sixteenfold way and hence the composite fermion description of half-integer quantum Hall plateaus. Given a close relation of the 16 orders, it is much harder to narrow down the list of possibilities to a single state. This subtle problem goes beyond the sort of questions one has to tackle at simpler filling factors like $\frac{1}{3}$. The current debate about the Pfaffian, PH-Pfaffian, and anti-Pfaffian orders in GaAs at $\nu = \frac{5}{2}$ illustrates this point [128].

One cannot help wondering whether all 16 topological orders of the sixteenfold way may be present in some physical systems. Only experiment can shed light on this question. This motivates a review of possible experimental signatures in this paper.

The PH-Pfaffian order gives rise to a curious situation. That topological order is compatible with the particle-hole (PH) symmetry [22], yet it appears that PH-symmetric Hamiltonians break the PH symmetry in their ground states [28–31]. On the other hand, disorder and Landau-level mixing break the PH symmetry of a Hamiltonian. The symmetry-from-no-symmetry principle [24] suggests that those symmetry-breaking effects stabilize the PH-symmetric order. Indeed, mechanisms [103–106] have been proposed for the stabilization of the PH-Pfaffian topological order by LLM and disorder. Moreover, existing coupled-wire constructions for the PH-Pfaffian order also break the particle-hole symmetry (see Ref. [97]). In fact, our coupled-stripe construction for getting the PH-Pfaffian order from Pfaffian stripes is rather similar to the stabilization of the PH-Pfaffian order by disorder in the mechanisms [104–106]. The coupled-stripe construction involves no disorder, but it breaks the PH symmetry in a way similar to how it is broken by disorder in those mechanisms [104–106]. This is another manifestation of the symmetry-from-no-symmetry principle [24] for the PH-Pfaffian liquids.

In conclusion, we give a uniform description of different proposed topological orders for the half-integer fractional quantum Hall states. The candidate orders can be seen as arising from Cooper pairing between composite fermions in different pairing channels. We introduce a mother-daughter relation between the topological orders, which relates them iteratively via particle-hole conjugation and neutral-mode flipping. The same mother-daughter relation allows us to iteratively construct wave functions and effective Hamiltonians for all orders. We also verify explicitly that all resulting topological orders belong to Kitaev's sixteenfold way [15]. This is used to predict experimental signatures of all 16 orders in multiple types of experiments, as summarized in Table VI.

ACKNOWLEDGMENTS

We acknowledge useful discussions with P. T. Zucker. This research was supported in part by the National Science Foundation under Grant No. DMR-1607451.

APPENDIX: FINITE-TEMPERATURE MACH-ZEHNDER INTERFEROMETRY

In Sec. V, we discussed experimental signatures of topological orders in Mach-Zehnder interferometry at zero temperature. In this Appendix, the discussion is generalized to finite-temperature systems on the basis of the kinetic equation approach [75,93].

1. Review of kinetic equations

We introduce the symbol $P_{s,i}(t)$ for the probability that the charge sq was transferred from source S1 to drain D2 during the time t. Here, q is the charge of the quasiparticle which dominates tunneling, and i labels the topological charge of drain D2 at the time t. The topological charge is not affected by the transfer of an integer number of electrons to D2 ($s \to s + ne/q$). The probability satisfies the following kinetic equation:

$$\frac{d}{dt}P_{l,i}(t) = \sum_{j=1}^{\mathcal{N}}[P_{l-1,j}(t)w^{+}_{j\to i} + P_{l+1,j}(t)w^{-}_{j\to i}] - \sum_{j=1}^{\mathcal{N}} P_{l,j}(t)(w^{+}_{i\to j} + w^{-}_{i\to j}). \tag{A1}$$

In the above equation, $\mathcal{N}$ labels the number of possible topological charges. The symbol $w_{i\to j}$ labels the transition rate from sector i to sector j. The superscript "+" corresponds to tunneling from the edge with the higher electrochemical potential to the edge with the lower electrochemical potential (edge 1 to edge 2 in Fig. 6). We call this type of tunneling "forward tunneling." At a nonzero temperature, thermal fluctuations allow backward tunneling from edge 2 to edge 1. The corresponding transition rates carry the superscript "−."

The calculation of $w_{i\to j}$ consists of two steps. First, we assume that the tunneling anyon and the initial topological charge i of the drain are in the fusion channel j. We compute the tunneling rate $p^{+}_{i\to j}$ under this assumption. On the second step, we multiply the outcome $p^{+}_{i\to j}$ of the first step by the probability of the fusion channel j. The bare tunneling rate $p^{-}_{j\to i}$ is defined in a similar way. It is related to the rate of the forward process by the detailed balance principle:

$$p^{-}_{j\to i} = \exp\left(-\frac{qV}{k_B T}\right)p^{+}_{i\to j}. \tag{A2}$$

Again, the above result must be multiplied by the probability of the fusion outcome i. Let x be the topological charge of the tunneling particle. The fusion probability of i and x into j is known from the algebraic theory of anyons [15,74,75,93]:

$$p^{j}_{ix} = N^{j}_{ix}\frac{d_j}{d_i d_x}, \tag{A3}$$

where N_{ix}^{j} is the fusion multiplicity and d_c labels the quantum dimension of anyon c. This fusion probability is independent of the temperature. As an example of its calculation, consider tunneling between the states $(-e/4, \sigma)$ and $(0, \psi)$. The fusion probability of forward tunneling $(-e/4 \to 0)$ equals $\frac{1}{2}$ since $\sigma \times \sigma = \psi + I$, $N_{\sigma\sigma}^{\psi} = 1$, $d_\psi = 1$, and $d_\sigma = \sqrt{2}$. However, the fusion probability from $(0, \psi)$ to $(-e/4, \sigma)$ for the backward tunneling is 1 since $\psi \times \sigma = \sigma$. The total transition rates are given by

$$w_{i\to j}^{+} = p_{\alpha x}^{\beta} p_{i\to j}^{+},\ w_{j\to i}^{-} = p_{\beta\bar{x}}^{\alpha} p_{j\to i}^{-}, \tag{A4}$$

where $\bar{x}$ is the antiparticle of x.

We introduce a generating function

$$f_i(z,t) = \sum_{n=-\infty}^{\infty} P_{k+ne/q,i}(t) z^{k+ne/q}. \tag{A5}$$

Here, k is uniquely determined by the topological sector i. In terms of f_i, the average charge transmitted during the time interval t and its variance are given by

$$\langle Q(t)\rangle = q\left(\frac{d}{dz}\sum_{i=1}^{\mathcal{N}} f_i\right)\Big|_{z=1} \tag{A6}$$

and

$$\langle \delta Q^2(t)\rangle = q^2\left(\frac{d}{dz} z \frac{d}{dz}\sum_{i=1}^{\mathcal{N}} f_i\right)\Big|_{z=1} - \langle Q(t)\rangle^2. \tag{A7}$$

From Eq. (A1) we obtain a kinetic equation for $f_i(z,t)$ as

$$\frac{d}{dt} f_i(z,t) = \sum_{j=1}^{\mathcal{N}}\left[z f_j(z,t) w_{j\to i}^{+} + \frac{1}{z} f_j(z,t) w_{j\to i}^{-}\right] - \sum_{j=1}^{\mathcal{N}} f_i(z,t)(w_{i\to j}^{+} + w_{i\to j}^{-}). \tag{A8}$$

The above equation can be written in the matrix form $\dot{\mathbf{f}}(z,t) = \mathbf{A}\cdot\mathbf{f}(z,t)$. At $z = 1$, the kinetic matrix $\mathbf{A}$ satisfies the Rohbrach theorem [145]. Therefore, all its eigenvalues are nonpositive at $z = 1$. Besides, one of the eigenvalues must be zero and nondegenerate. We denote it as $\lambda(z)$. This eigenvalue dominates the long-term behavior of the solution of Eq. (A8). With this idea, the tunneling current and the Fano factor can be evaluated as

$$I = \lim_{t\to\infty}\frac{\langle Q(t)\rangle}{t} = q\lambda'(z)\big|_{z=1} \tag{A9}$$

and

$$e^* = \lim_{t\to\infty}\frac{\langle \delta Q^2(t)\rangle}{\langle Q(t)\rangle} = q\left[1 + \frac{\lambda''(z)\big|_{z=1}}{\lambda'(z)|_{z=1}}\right]. \tag{A10}$$

In practice, it is not straightforward to obtain $\lambda(z)$. Nevertheless, $\lambda'(1)$ and $\lambda''(1)$ can be determined from the characteristic equation $\det[\mathbf{A}(z) - \lambda(z)\mathbf{I}] = 0$ [93]. Suppose the characteristic equation takes the form $C_0(z) + C_1(z)\lambda(z) + C_2(z)\lambda(z)^2 + \cdots = 0$. Using the condition that $\lambda(1) = 0$ and the product rule, we have

$$\lambda'(1) = -\frac{C_0'(1)}{C_1(1)}, \tag{A11}$$

$$\lambda''(1) = -\frac{C_0''(1) + 2C_1'(1)\lambda'(1) + 2C_2(1)\lambda'(1)^2}{C_1(1)}. \tag{A12}$$

From the above results, the tunneling current and the Fano factor at finite temperatures can be evaluated systematically.

2. $e/4$-quasiparticle tunneling

Now, we evaluate the tunneling current and the Fano factor at a finite temperature when the tunneling process is dominated by charge-$e/4$ quasiparticles. We focus on non-Abelian orders. In this case, there are $\mathcal{N} = 6$ superselection sectors as depicted in Fig. 7. For simplicity, we separate the kinetic matrix into three pieces: $\mathbf{A} = \mathbf{A}_F + \mathbf{A}_B + \mathbf{A}_L$. The first matrix corresponds to forward tunneling from state j to state i. By ordering the superselection sectors as $(-e/4, \sigma)$, $(0, \psi)$, $(0, I)$, $(e/4, \sigma)$, $(e/2, \psi)$, and $(e/2, I)$, we have

$$\mathbf{A}_F = z\begin{pmatrix} 0 & 0 & 0 & 0 & p\left(-\frac{\pi}{2}\right) & p\left(\frac{\pi}{2}\right) \\ p_1/2 & 0 & 0 & 0 & 0 & 0 \\ p_3/2 & 0 & 0 & 0 & 0 & 0 \\ 0 & p(\pi) & p(0) & 0 & 0 & 0 \\ 0 & 0 & 0 & p_2/2 & 0 & 0 \\ 0 & 0 & 0 & p_4/2 & 0 & 0 \end{pmatrix}. \tag{A13}$$

The symbols $p_{\mathbf{k}}$ and $p(\phi_s)$ are defined in Sec. V. The second matrix represents backward tunneling from state j to state i:

$$\mathbf{A}_B = \frac{1}{z}\mu\begin{pmatrix} 0 & p_1 & p_3 & 0 & 0 & 0 \\ 0 & 0 & 0 & p(\pi)/2 & 0 & 0 \\ 0 & 0 & 0 & p(0)/2 & 0 & 0 \\ 0 & 0 & 0 & 0 & p_2 & p_4 \\ p\left(-\frac{\pi}{2}\right)/2 & 0 & 0 & 0 & 0 & 0 \\ p\left(\frac{\pi}{2}\right)/2 & 0 & 0 & 0 & 0 & 0 \end{pmatrix}, \tag{A14}$$

where $\mu = e^{-eV/(4k_BT)}$. Lastly, $\mathbf{A}_L$ is the diagonal piece of the kinetic matrix with the following matrix elements:

$$\begin{aligned}
(\mathbf{A}_L)_{11} &= -\left[\frac{p_1}{2} + \frac{p_3}{2}\right] - \frac{\mu}{2}\left[p\left(-\frac{\pi}{2}\right) + p\left(\frac{\pi}{2}\right)\right], \\
(\mathbf{A}_L)_{22} &= -p(\pi) - \mu p_1, \\
(\mathbf{A}_L)_{33} &= -p(0) - \mu p_3, \\
(\mathbf{A}_L)_{44} &= -\left[\frac{p_2}{2} + \frac{p_4}{2}\right] - \frac{\mu}{2}\left[p(\pi) + p(0)\right], \\
(\mathbf{A}_L)_{55} &= -p\left(-\frac{\pi}{2}\right) - \mu p_2, \\
(\mathbf{A}_L)_{66} &= -p\left(\frac{\pi}{2}\right) - \mu p_4.
\end{aligned} \tag{A15}$$

Using Eqs. (A9) and (A11), we obtain the generalization of Eqs. (87)–(90) to a finite temperature. From the top to the bottom, $\nu_C = 1, 3, 5, 7 \pmod 8$:

$$I_{e/4} = \frac{er}{4}(|\Gamma_1|^2 + |\Gamma_2|^2)(1-\mu)\left[\frac{(1+\mu)^2(1-s^2) + \frac{s^4}{8}(\mu^2+6\mu+1) - \frac{s^4}{8}(\mu-1)^2\cos 4\gamma}{(1+\mu)^2\left(1-\frac{3s^2}{4}\right) + \frac{s^4}{16}(\mu^2+6\mu+1) - \frac{s^4}{16}[(\mu-1)^2\cos 4\gamma - (\mu^2-1)\sin 4\gamma]}\right], \tag{A16}$$

$$I_{e/4} = \frac{er}{4}(|\Gamma_1|^2 + |\Gamma_2|^2)(1-\mu)\left[\frac{1 - s^2 + \frac{s^4}{4}\sin^2 2\gamma}{1-\frac{s^2}{2}}\right] = I_{e/4}(0)[1 - e^{-eV/(4k_BT)}], \tag{A17}$$

$$I_{e/4} = \frac{er}{4}(|\Gamma_1|^2 + |\Gamma_2|^2)(1-\mu)\left[\frac{(1+\mu)^2(1-s^2) + \frac{s^4}{8}(\mu^2+6\mu+1) - \frac{s^4}{8}(\mu-1)^2\cos 4\gamma}{(1+\mu)^2\left(1-\frac{3s^2}{4}\right) + \frac{s^4}{16}(\mu^2+6\mu+1) - \frac{s^4}{16}[(\mu-1)^2\cos 4\gamma + (\mu^2-1)\sin 4\gamma]}\right], \tag{A18}$$

$$I_{e/4} = \frac{er}{4}(|\Gamma_1|^2 + |\Gamma_2|^2)(1-\mu) = I_{e/4}(0)[1 - e^{-eV/(4k_BT)}]. \tag{A19}$$

Notice that the zero-temperature results can be recovered in all cases by setting $\mu = 0$. Note also that the coefficients r and s can contain an additional dependence on the voltage and temperature. For Abelian topological orders, the calculation is essentially the same. However, the results are too lengthy to be displayed here.

Fano factor for the PH-Pfaffian order

In principle, the Fano factor can be calculated from Eqs. (A10), (A11), and (A12). However, a simple analytic expression only exists when $\nu_C \equiv 7 \pmod 8$. This covers the PH-Pfaffian case. One can show [136] that

$$e^*(T) = \frac{e}{2}\mathrm{csch}\left(\frac{eV}{4k_BT}\right) + e^*(0)\tanh\left(\frac{eV}{8k_BT}\right), \tag{A20}$$

where $e^*(0)$ is given by Eq. (100), and s in Eq. (100) may depend on T and V.

3. $e/2$-quasiparticle tunneling

If the tunneling process is dominated by $e/2$ quasiparticles, the calculation simplifies dramatically. There are only two superselection sectors as shown in Fig. 8. We limit our discussion to the case, represented in the left panel of Fig. 8. From Eq. (A8) with $\mathcal{N} = 2$, one can derive the following kinetic matrix:

$$\mathbf{A} = \begin{pmatrix} -p(-\frac{\pi}{2}) - \mu' p(\frac{\pi}{2}) & zp(\frac{\pi}{2}) + \frac{1}{z}\mu' p(-\frac{\pi}{2}) \\ zp(-\frac{\pi}{2}) + \frac{1}{z}\mu' p(\frac{\pi}{2}) & -p(\frac{\pi}{2}) - \mu' p(-\frac{\pi}{2}) \end{pmatrix}. \tag{A21}$$

Here, $\mu' = e^{-eV/(2k_BT)}$. Following the previous procedure, we determine the tunneling current at a finite temperature as

$$I_{e/2}(T) = I_{e/2}(0)[1 - e^{-eV/(2k_BT)}], \tag{A22}$$

where $I_{e/2}(0)$ is given in Eq. (91). Furthermore, the Fano factor at a finite temperature is evaluated as

$$e^*_{e/2}(T) = e\,\mathrm{csch}\left(\frac{eV}{2k_BT}\right) + e^*_{e/2}(0)\tanh\left(\frac{eV}{4k_BT}\right). \tag{A23}$$

As always, r and s in the expressions for $I_{e/2}(0)$ and $e^*_{e/2}(0)$ may depend on T and V.

[1] D. C. Tsui, H. L. Stormer, and A. C. Gossard, Phys. Rev. Lett. **48**, 1559 (1982).
[2] R. Willett, J. P. Eisenstein, H. L. Störmer, D. C. Tsui, A. C. Gossard, and J. H. English, Phys. Rev. Lett. **59**, 1776 (1987).
[3] W. Pan, J.-S. Xia, V. Shvarts, D. E. Adams, H. L. Stormer, D. C. Tsui, L. N. Pfeiffer, K. W. Baldwin, and K. W. West, Phys. Rev. Lett. **83**, 3530 (1999).
[4] G. Moore and N. Read, Nucl. Phys. B **360**, 362 (1991).
[5] X. G. Wen, Phys. Rev. Lett. **66**, 802 (1991).
[6] M. Greiter, X. G. Wen, and F. Wilczek, Nucl. Phys. B **374**, 567 (1992).
[7] C. Nayak and F. Wilczek, Nucl. Phys. B **479**, 529 (1996).
[8] A. Y. Kitaev, Ann. Phys. (NY) **303**, 2 (2003).
[9] C. Nayak, S. H. Simon, A. Stern, M. Freedman, and S. Das Sarma, Rev. Mod. Phys. **80**, 1083 (2008).
[10] M. Z. Hasan and C. L. Kane, Rev. Mod. Phys. **82**, 3045 (2010).
[11] X.-L. Qi and S.-C. Zhang, Rev. Mod. Phys. **83**, 1057 (2011).
[12] M. Sato and Y. Ando, Rep. Prog. Phys. **80**, 076501 (2017).
[13] J. K. Jain, *Composite Fermions* (Cambridge University Press, New York, 2007).
[14] N. Read and D. Green, Phys. Rev. B **61**, 10267 (2000).
[15] A. Y. Kitaev, Ann. Phys. (NY) **321**, 2 (2006).
[16] Y. W. Suen, L. W. Engel, M. B. Santos, M. Shayegan, and D. C. Tsui, Phys. Rev. Lett. **68**, 1379 (1992).
[17] J. P. Eisenstein, G. S. Boebinger, L. N. Pfeiffer, K. W. West, and S. He, Phys. Rev. Lett. **68**, 1383 (1992).
[18] B. I. Halperin, Helv. Phys. Acta **56**, 75 (1983).
[19] D. Yoshioka, A. H. MacDonald, and S. M. Girvin, Phys. Rev B **39**, 1932 (1989).
[20] S. He, S. Das Sarma, and X. C. Xie, Phys. Rev. B **47**, 4394 (1993).

[21] M. R. Peterson and S. Das Sarma, Phys. Rev. B **81**, 165304 (2010).
[22] D. T. Son, Phys. Rev. X **5**, 031027 (2015).
[23] D. T. Son, Prog. Theor. Exp. Phys. **2016**, 12C103 (2016).
[24] P. T. Zucker and D. E. Feldman, Phys. Rev. Lett. **117**, 096802 (2016).
[25] S.-S. Lee, S. Ryu, C. Nayak, and M. P. A. Fisher, Phys. Rev. Lett. **99**, 236807 (2007).
[26] L. Fidkowski, X. Chen, and A. Vishwanath, Phys. Rev. X **3**, 041016 (2013).
[27] P. Bonderson, C. Nayak, and X.-L. Qi, J. Stat. Mech. (2013) P09016.
[28] R. H. Morf, Phys. Rev. Lett. **80**, 1505 (1998).
[29] K. Pakrouski, M. R. Peterson, T. Jolicoeur, V. W. Scarola, C. Nayak, and M. Troyer, Phys. Rev. X **5**, 021004 (2015).
[30] M. P. Zaletel, R. S. K. Mong, F. Pollmann, and E. H. Rezayi, Phys. Rev. B **91**, 045115 (2015).
[31] E. H. Rezayi, Phys. Rev. Lett. **119**, 026801 (2017) and references therein.
[32] W. Luo and T. Chakraborty, Phys. Rev. B **96**, 081108(R) (2017).
[33] B. Yang, Phys. Rev. B **98**, 201101(R) (2018).
[34] M. Levin, B. I. Halperin, and B. Rosenow, Phys. Rev. Lett. **99**, 236806 (2007).
[35] X. Lin, C. Dillard, M. A. Kastner, L. N. Pfeiffer, and K. W. West, Phys. Rev. B **85**, 165321 (2012).
[36] S. Baer, C. Rössler, T. Ihn, K. Ensslin, C. Reichl, and W. Wegscheider, Phys. Rev. B **90**, 075403 (2014).
[37] H. Fu, P. Wang, P. Shan, L. Xiong, L. N. Pfeiffer, K. West, M. A. Kastner, and X. Lin, Proc. Natl. Acad. Sci. USA **113**, 12386 (2016).
[38] G. Yang and D. E. Feldman, Phys. Rev. B **88**, 085317 (2013).
[39] G. Yang and D. E. Feldman, Phys. Rev. B **90**, 161306(R) (2014).
[40] W. Pan, A. Serafin, J. S. Xia, L. Yin, N. S. Sullivan, K. W. Baldwin, K. W. West, L. N. Pfeiffer, and D. C. Tsui, Phys. Rev. B **89**, 241302(R) (2014).
[41] N. Samkharadze, D. Ro, L. N. Pfeiffer, K. W. West, and G. A. Csáthy, Phys. Rev. B **96**, 085105 (2017).
[42] J. P. Eisenstein, K. B. Cooper, L. N. Pfeiffer, and K. W. West, Phys. Rev. Lett. **88**, 076801 (2002).
[43] Y. Liu, J. Shabani, D. Kamburov, M. Shayegan, L. N. Pfeiffer, K. W. West, and K. W. Baldwin, Phys. Rev. Lett. **107**, 266802 (2011).
[44] J. Falson, D. Maryenko, B. Friess, D. Zhang, Y. Kozuka, A. Tsukazaki, J. H. Smet, and M. Kawasaki, Nat. Phys. **11**, 347 (2015).
[45] J. Falson, D. Tabrea, D. Zhang, I. Sodemann, Y. Kozuka, A. Tsukazaki, M. Kawasaki, K. von Klitzing, and J. H. Smet, Sci. Adv. **4**, eaat8742 (2018).
[46] Y.-H. Wu, T. Shi, and J. K. Jain, Nano Lett. **17**, 4643 (2017).
[47] Y. Kim, A. C. Balram, T. Taniguchi, K. Watanabe, J. K. Jain, and J. H. Smet, Nat. Phys. **15**, 154 (2019).
[48] Y. Kasahara, T. Ohnishi, Y. Mizukami, O. Tanaka, S. Ma, K. Sugii, N. Kurita, H. Tanaka, J. Nasu, Y. Motome, T. Shibauchi, and Y. Matsuda, Nature (London) **559**, 227 (2018).
[49] M. Dolev, M. Heiblum, V. Umansky, A. Stern, and D. Mahalu, Nature (London) **452**, 829 (2008).
[50] R. L. Willett, L. N. Pfeiffer, and K. W. West, Proc. Natl. Acad. Sci. USA **106**, 8853 (2009).
[51] M. Dolev, Y. Gross, Y. C. Chung, M. Heiblum, V. Umansky, and D. Mahalu, Phys. Rev. B **81**, 161303(R) (2010).
[52] R. L. Willett, L. N. Pfeiffer, and K. W. West, Phys. Rev. B **82**, 205301 (2010).
[53] V. Venkatachalam, A. Yacoby, L. Pfeiffer, and K. West, Nature (London) **469**, 185 (2011).
[54] I. P. Radu, J. B. Miller, C. M. Marcus, M. A. Kastner, L. N. Pfeiffer, and K. W. West, Science **320**, 899 (2008).
[55] L. Tiemann, G. Gamez, N. Kumada, and K. Muraki, Science **335**, 828 (2012).
[56] M. Stern, B. A. Piot, Y. Vardi, V. Umansky, P. Plochocka, D. K. Maude, and I. Bar-Joseph, Phys. Rev. Lett. **108**, 066810 (2012).
[57] U. Wurstbauer, K. W. West, L. N. Pfeiffer, and A. Pinczuk, Phys. Rev. Lett. **110**, 026801 (2013).
[58] Md. Shafayat Hossain, M. K. Ma, M. A. Mueed, L. N. Pfeiffer, K. W. West, K. W. Baldwin, and M. Shayegan, Phys. Rev. Lett. **120**, 256601 (2018).
[59] M. Stern, P. Plochocka, V. Umansky, D. K. Maude, M. Potemski, and I. Bar-Joseph, Phys. Rev. Lett. **105**, 096801 (2010).
[60] X.-G. Wen, *Quantum Field Theory of Many-Body Systems: From the Origin of Sound to an Origin of Light and Electrons* (Oxford University Press, Oxford, 2004).
[61] B. J. Overbosch and X.-G. Wen, arXiv:0804.2087.
[62] M. Banerjee, M. Heiblum, V. Umansky, D. E. Feldman, Y. Oreg, and A. Stern, Nature (London) **559**, 205 (2018).
[63] C. L. Kane and M. P. A. Fisher, Phys. Rev. B **55**, 15832 (1997).
[64] A. Cappelli, M. Huerta, and G. R. Zemba, Nucl. Phys. B **636**, 568 (2002).
[65] K. K. W. Ma and D. E. Feldman, Phys. Rev. B **99**, 085309 (2019).
[66] D. E. Feldman and F. Li, Phys. Rev. B **78**, 161304(R) (2008).
[67] A. Bid, N. Ofek, H. Inoue, M. Heiblum, C. L. Kane, V. Umansky, and D. Mahalu, Nature (London) **466**, 585 (2010).
[68] M. Dolev, Y. Gross, R. Sabo, I. Gurman, M. Heiblum, V. Umansky, and D. Mahalu, Phys. Rev. Lett. **107**, 036805 (2011).
[69] C. Wang and D. E. Feldman, Phys. Rev. B **84**, 235315 (2011).
[70] Y. Gross, M. Dolev, M. Heiblum, V. Umansky, and D. Mahalu, Phys. Rev. Lett. **108**, 226801 (2012).
[71] C. Wang and D. E. Feldman, Phys. Rev. Lett. **110**, 030602 (2013).
[72] A. Stern and B. I. Halperin, Phys. Rev. Lett. **96**, 016802 (2006).
[73] P. Bonderson, A. Kitaev, and K. Shtengel, Phys. Rev. Lett. **96**, 016803 (2006).
[74] D. E. Feldman and A. Kitaev, Phys. Rev. Lett. **97**, 186803 (2006).
[75] D. E. Feldman, Y. Gefen, A. Kitaev, K. T. Law, and A. Stern, Phys. Rev. B **76**, 085333 (2007).
[76] V. V. Ponomarenko and D. V. Averin, Phys. Rev. Lett. **99**, 066803 (2007).
[77] V. V. Ponomarenko and D. V. Averin, Phys. Rev. B **82**, 205411 (2010).
[78] C. Wang and D. E. Feldman, Phys. Rev. B **82**, 165314 (2010).
[79] G. Yang, Phys. Rev. B **91**, 115109 (2015).
[80] C. de C. Chamon, D. E. Freed, S. A. Kivelson, S. L. Sondhi, and X. G. Wen, Phys. Rev. B **55**, 2331 (1997).
[81] C. L. Kane, Phys. Rev. Lett. **90**, 226802 (2003).

[82] S. B. Chung and M. Stone, Phys. Rev. B **73**, 245311 (2006).
[83] P. Bonderson, K. Shtengel, and J. K. Slingerland, Phys. Rev. Lett. **97**, 016401 (2006).
[84] R. Ilan, E. Grosfeld, and A. Stern, Phys. Rev. Lett. **100**, 086803 (2008).
[85] W. Bishara, P. Bonderson, C. Nayak, K. Shtengel, and J. K. Slingerland, Phys. Rev. B **80**, 155303 (2009).
[86] R. Ilan, E. Grosfeld, K. Schoutens, and A. Stern, Phys. Rev. B **79**, 245305 (2009).
[87] P. Bonderson, C. Nayak, and K. Shtengel, Phys. Rev. B **81**, 165308 (2010).
[88] A. Stern, B. Rosenow, R. Ilan, and B. I. Halperin, Phys. Rev. B **82**, 085321 (2010).
[89] K. T. Law, D. E. Feldman, and Y. Gefen, Phys. Rev. B **74**, 045319 (2006).
[90] S. An, P. Jiang, H. Choi, W. Kang, S. H. Simon, L. N. Pfeiffer, K. W. West, and K. W. Baldwin, arXiv:1112.3400.
[91] B. Rosenow and S. H. Simon, Phys. Rev. B **85**, 201302(R) (2012).
[92] E. V. Deviatov, S. V. Egoro, G. Biasiol, and L. Sorba, Europhys. Lett. **100**, 67009 (2013).
[93] K. T. Law, Phys. Rev. B **77**, 205310 (2008).
[94] G. Campagnano, O. Zilberberg, I. V. Gornyi, D. E. Feldman, A. C. Potter, and Y. Gefen, Phys. Rev. Lett. **109**, 106802 (2012).
[95] Y. Ji, Y. C. Chung, D. Sprinzak, M. Heiblum, D. Mahalu, and H. Shtrikman, Nature (London) **422**, 415 (2003).
[96] J. C. Y. Teo and C. L. Kane, Phys. Rev. B **89**, 085101 (2014).
[97] C. L. Kane, A. Stern, and B. I. Halperin, Phys. Rev. X **7**, 031009 (2017).
[98] Y. Fuji and A. Furusaki, Phys. Rev. B **99**, 035130 (2019).
[99] W. Bishara and C. Nayak, Phys. Rev. B **80**, 121302(R) (2009).
[100] M. R. Peterson and C. Nayak, Phys. Rev. B **87**, 245129 (2013).
[101] S. H. Simon and E. H. Rezayi, Phys. Rev. B **87**, 155426 (2013).
[102] I. Sodemann and A. H. MacDonald, Phys. Rev. B **87**, 245425 (2013).
[103] L. Antonić, J. Vučičević, and M. V. Milovanović, Phys. Rev. B **98**, 115107 (2018).
[104] D. F. Mross, Y. Oreg, A. Stern, G. Margalit, and M. Heiblum, Phys. Rev. Lett. **121**, 026801 (2018).
[105] C. Wang, A. Vishwanath, and B. I. Halperin, Phys. Rev. B **98**, 045112 (2018).
[106] B. Lian and J. Wang, Phys. Rev. B **97**, 165124 (2018).
[107] W. Zhu and D. N. Sheng, arXiv:1809.04776.
[108] S. M. Girvin and T. Jach, Phys. Rev. B **29**, 5617 (1984).
[109] S. M. Girvin, arXiv:cond-mat/9907002.
[110] R. L. Willett, K. W. West, and L. N. Pfeiffer, Phys. Rev. Lett. **88**, 066801 (2002).
[111] V. W. Scarola, K. Park, and J. K. Jain, Nature (London) **406**, 863 (2000).
[112] D. A. Ivanov, Phys. Rev. Lett. **86**, 268 (2001).
[113] P. Fendley, M. P. A. Fisher, and C. Nayak, Phys. Rev. B **75**, 045317 (2007).
[114] J. Dubail and N. Read, Phys. Rev. Lett. **107**, 157001 (2011).
[115] X. G. Wen and A. Zee, Phys. Rev. B **46**, 2290 (1992).
[116] "Counterclockwise" means counterclockwise when looking in the direction of the magnetic field. We will generally assume that negatively charged electrons move in a magnetic field, pointing down.
[117] Th. Jolicoeur, Phys. Rev. Lett. **99**, 036805 (2007).
[118] C. L. Kane and M. P. A. Fisher, Phys. Rev. B **51**, 13449 (1995).
[119] J. K. Jain, Phys. Rev. B **40**, 8079(R) (1989).
[120] T. H. Hansson, M. Hermanns, S. H. Simon, and S. F. Viefers, Rev. Mod. Phys. **89**, 025005 (2017).
[121] R. V. Mishmash, D. F. Mross, J. Alicea, and O. I. Motrunich, Phys. Rev. B **98**, 081107(R) (2018).
[122] Indeed, the wave function before a projection has the correct angular momentum. This implies the right electron density and shift after the projection, even if the projection is only performed once at the last step. We expect the topological order to also be correct.
[123] Note that the order and disorder operators σ and μ in the Ising chiral CFT have the same $h = \frac{1}{16}$.
[124] P. A. Russell, F. F. Ouali, N. P. Hewett, and L. J. Challis, Surf. Sci. **229**, 54 (1990).
[125] U. Klaß, W. Dietsche, and K. V. Klitzing, Z. Phys. B **82**, 351 (1991).
[126] T. Ise, H. Akera, and H. Suzuura, J. Phys. Soc. Jpn. **74**, 259 (2005).
[127] M. Banerjee, M. Heiblum, A. Rosenblatt, Y. Oreg, D. E. Feldman, A. Stern, and V. Umansky, Nature (London) **545**, 75 (2017).
[128] D. E. Feldman, Phys. Rev. B **98**, 167401 (2018).
[129] E. Papa and A. H. MacDonald, Phys. Rev. Lett. **93**, 126801 (2004).
[130] B. Rosenow and B. I. Halperin, Phys. Rev. Lett. **88**, 096404 (2002).
[131] K. Yang, Phys. Rev. Lett. **91**, 036802 (2003).
[132] M. Carrega, D. Ferraro, A. Braggio, N. Magnoli, and M. Sassetti, Phys. Rev. Lett. **107**, 146404 (2011).
[133] A. Seidel and K. Yang, Phys. Rev. B **80**, 241309(R) (2009).
[134] C. Wang and D. E. Feldman, Phys. Rev. B **81**, 035318 (2010).
[135] N. Jiang and X. Wan, AAPPS Bulletin **29**, 58 (2019).
[136] P. T. Zucker, PhD. dissertation, Brown University, 2017.
[137] Adding $(e, 0)$ to the drain shifts all interference phases by π. This shift can be ignored if one identifies the states $(ne/4, a)$ and $([n + 4]e/4, a + \psi)$ of the drain.
[138] N. Byers and C. N. Yang, Phys. Rev. Lett. **7**, 46 (1961).
[139] S. L. Sondhi and K. Yang, Phys. Rev. B **63**, 054430 (2001).
[140] C. L. Kane, R. Mukhopadhyay, and T. C. Lubensky, Phys. Rev. Lett. **88**, 036401 (2002).
[141] M. Barkeshli, M. Mulligan, and M. P. A. Fisher, Phys. Rev. B **92**, 165125 (2015).
[142] M. Mulligan, S. Raghu, and M. P. A. Fisher, Phys. Rev. B **94**, 075101 (2016).
[143] X. Wan and K. Yang, Phys. Rev. B **93**, 201303(R) (2016).
[144] M. Greiter, X. G. Wen, and F. Wilczek, Phys. Rev. Lett. **66**, 3205 (1991).
[145] E. B. Fel'dman, Theor. Exp. Chem. **10**, 645 (1976).